CCFE
CULHAM CENTRE FOR FUSION ENERGY

UK Atomic Energy Authority

UKAEA-CCFE-PR(20)16

Mike Fursdon, Jeong-Ha You

# Towards reliable design-by-analysis for divertor plasma facing components – guidelines for inelastic assessment (part II: irradiated)

# Towards reliable design-by-analysis for divertor plasma facing components – guidelines for inelastic assessment (part II: irradiated)

Mike Fursdon, Jeong-Ha You

This is a preprint of a paper submitted for publication in
Fusion Engineering and Design

# Towards reliable design-by-analysis for divertor plasma facing components – guidelines for inelastic assessment (part II: irradiated)

M Fursdon[1], J-H You[2]

1 CCFE, Culham Science Centre, Abingdon, OX14 3DB, UK,
2 Max-Planck-Institut für Plasmaphysik, Boltzmannstr. 2, 85748 Garching, Germany,

Email: mike.fursdon@ukaea.uk

Keywords: plasma facing component, structural integrity analysis, inelastic, elastoplastic, divertor, irradiated

## Abstract.

This paper gives guidelines for assessing the structural integrity of plasma facing components (PFC)when irradiated to the levels expected in DEMO after two full power years. The paper is part 2 of a 3-part paper describing the EuroFusion DEMO Divertor group (WPDIV) Inelastic Analysis procedure (IAP), created to improve the assessment of PFCs, and specifically those constructed from tungsten armour cooled by CuCrZr heat sink (with Copper interlayer). The paper presents a brief review of the limited relevant irradiated materials data on material properties (thermal conductivity, swelling and stress-strain curves) and materials limit data (rupture-strain, fracture-toughness and fatigue strength). The data is used in an example structural integrity assessment estimate of an ITER-like divertor "monoblock" PFC (tungsten block with through CuCrZr pipe) when irradiated to ~13dpa (CuCrZr) & ~ 4dp (tungsten). The assessment uses IAP methodologies outlined in the IAP part 1 paper to determine the susceptibility of the design to failure by exhaustion-of-ductility, fast-fracture, fatigue and ratcheting in the CuCrZr pipe, exhaustion of ductility in the copper interlayer and brittle fracture in the tungsten armour. These methodologies ensure that contributions from changes in both material limit-levels and material properties are included. The paper documents the extrapolations required to extend the existing irradiated materials data to the expected dpa and temperature range. The assessment exposes significant shortfalls in the monoblock type design in coping with the drastic reduction in Copper ductility and tungsten strength caused by irradiation. This illustrates that maintaining structural integrity when irradiated poses a far more stringent constraint on a PFC design than the un-irradiated condition, and as such should be given priority in future design studies. Although the prime aim of the paper is to present assessment methodologies, it also helps identify the key gaps in irradiated materials property data (and emphasise the severe need for a fully populating irradiated materials data-base).

# 1 Introduction

One of many challenges confronting the design of the DEMO fusion power plant is the development of plasma facing components (PFC) capable of withstanding the high flux loads (HHF) and high irradiation levels expected in the divertor. The challenge is exacerbated by the lack of a reliable method of calculating the "performance" of proposed designs for this environment, in terms of their structural integrity. This means that designs must be validated by testing (Hirai [1]), effectively forcing a process of design-by-experiment.

To improve the reliability of PFC structural integrity assessment calculations, EUROfusion's divertor design development group (WPDIV) have developed an analysis procedure specifically for divertor PFCs. This inelastic analysis Procedure (IAP) as it is known, provides details of analysis methodologies and preferred analysis design rules overcoming some of the difficulties identified in the current assessment methods. A full description the IAP methodologies and rules can be found in part 1 of this paper [2].

The part 1 paper also includes an example assessment of a typical divertor PFC design to illustrate how the IAP is applied. The design assessed in the example comprises a tungsten armour block with through CuCrZr pipe joined via a copper interlayer (as shown in Figure 1). This is the style of component being considered by ITER and DEMO, and much test data exists. The example analysis shows in part how the calculation may be used to supplement or replace validation test data.

However, neither the example assessment, nor the validation test data that exists, gives a full picture of expected PFC in-service performance. This is because they do not take account of the detrimental effect of irradiation. In DEMO these effects are expected to be significant: In the divertor the peak irradiation dose is predicted to be circa 6.5 dpa in the Cu/*CuCrZr* tube and 2 dpa in the W armour per full power year (fpy) (You [3]). "This continual irradiation of fast neutrons can produce crystal defects and transmutation products e.g. helium gas or brittle intermetallic phases (W/Re) in materials leading to embrittlement and other detrimental effects like reduction of heat conductivity". This means that, potentially irradiation creates the most onerous condition, and moreover the current practice of testing just the unirradiated component provides a false indicator of the full in-service "performance". This performance can only be determined by an assessment of the PFC in both its irradiated and unirradiated condition.

In the current stage of the DEMO program, this need for both pre & post irradiation life assessment exposes the weakness of the current design-by-experiment method. DEMO is currently in its pre-concept stage, typically involving numerous concept designs and a variety of design optimisation studies. In these circumstances, trying to validate pre & post irradiation performance by experiment is impractical, and emphasises the need for a reliable designs-by-analysis method; particularly a method capable of assessing the irradiated case.

This paper aims to show that the IAP can be used in part to fulfil this function, by at least allowing an estimate of irradiated PFC performance to be made. This is achieved by presenting an example assessment. Moreover, when combined with the assessment of the unirradiated performance, as demonstrated in the part 1 paper, the desired full-life assessment is partially realised.

Currently it is only possible to make an estimate of irradiated performance, because the available irradiated materials data is scarce. To make the estimate it is necessary to extrapolate existing data significantly. This part II paper describes the extent of relevant irradiated materials data and presents some of the extrapolation methods used to allow an assessment to be made.

In all the paper has four main objectives:

1. Show how that the IAP can be used to estimate the full-life (pre & post irradiation) structural integrity "performance" of PFCs.
2. Identify and highlight the significant gaps in the currently available irradiated materials data.
3. Show that testing of the unirradiated component does not provide a good indication of full life performance.
4. Give a critical review of the irradiated structural integrity of current benchmark "monoblock" divertor PFC design.

## 1.2 *Assessment methodology*

### 1.2.1 Recap of general IAP assessment methodology

Like most current design codes, the IAP determines the susceptibility of a design to a number of damage mechanisms. In ductile materials at low temperatures (i.e. where creep is deemed insignificant), four mechanisms are assessed: exhaustion-of-ductility, fast-fracture, fatigue and ratcheting. For the first three, the limiting level of damage is measured by the materials true-strain-at-rupture, fracture-toughness, and fatigue strain-life-curves respectively. The assessment compares the calculated damage incurred under the applied PFC loads, against limit levels using the criteria detailed in the part 1 paper. Ratcheting is assessed be explicit demonstration of stable cyclic displacement/strain behaviour.

The comparison of damage vs limit is achieved using usage-fractions (for example calculated strain divided by true strain at rupture). In some cases, such as fatigue, usage may need to be summed for all the load cases, resulting from normal operating cycles, and upset loads. The total usage should always be less than one. Usage fractions are particularly useful when both the level of damage and the limit level are variable, because of various factors including local variations in irradiation damage stress/strain level and temperature. Contour plots are used show local usage which aids identification of areas of concern which may not be coincident with maximum stress or strain.

To increase the effectiveness of the assessment, the IAP also includes proposed rules for the nominally brittle armour material

of PFC's. This is done specifically with the aim of capturing the typical failures seen in existing HHF tests such as deep cracking. For these materials the IAP currently uses criterion based on UTS, and fatigue in recrystalised material (leading to deep cracking), but further rules are being investigated.

The structural integrity assessment of PFCs is complicated by their multilateral construction, with dissimilar yield strengths and dissimilar coefficients of thermal expansion of the component materials. For this reason, the IAP uses inelastic analysis methods to ensure the distribution of loads across the subcomponents are correctly yield limited. Also, the differing thermal expansion of the component materials has been shown [4] to cause large through-thickness residual stress generated during PFC manufacture. To take account of these residual stresses, the IAP includes additional analysis steps to simulate approximately the manufacturing cycle (as developed by Li [5] and Miskiewicz[6]).

### 1.2.2 Irradiation specific methodologies

The assessment of irradiated components (as opposed to the un-irradiated case) is achieved, in part, by carrying out the standard IAP assessment process, but with modified irradiated materials data. Two aspects or irradiation effects are included: Firstly, the change in the materials damage limits are applied for each of the damage mechanisms (exhaustion of ductility true strain at rupture), fast fracture (fracture toughness $K_{1c}$), fatigue (e-N data) and ratcheting ($NA$)[(1)]. Secondly modification of material properties are also applied, in this case specifically: thermal conductivity, density (swelling) and materials strength/modulus as captured by modified stress-strain curves (necessary for the inelastic analysis methods used).

(1) No explicit limiting material property is defined for ratcheting although the effect of irradiation in ratcheting is captured implicitly by the materials change in stress strain characteristics)

The IAP assessment also includes two additional methodologies directed specifically at irradiated component assessment. Primarily these are added so that the combined effects of both pre and post irradiation effects are captured, particularly where damage usages in each phase might be significantly different. The first methodology aims to capture approximately and within a single simulation, the effect of the evolving material properties caused by irradiation. This is done by first using the previously described unirradiated "load" steps (of manufacture, standby and "normal" loads) using unirradiated material properties. These are then followed by additional cycles where the material properties are changed to the revised irradiated properties [in ANSYS using the MPCHG]. This methodology primarily aims to give an approximate picture of the effects caused by the accumulation of strains throughout the various phases of component life.

The second "irradiation specific" methodology deals with the accumulation of damage in "pre" and "post-irradiation" phases of operations. It is assumed that if extensive damage occurs before irradiation then this might reduce the ability of a material to cope with subsequent damage occurring after irradiation. To the authors knowledge there is no data available to confirm this effect, so it is proposed that this use of damage is proportionate. Hence, in the case of ductility usage (for example): if 50% ductility usage ($U_{d\text{-}pre}$) occurs before irradiation, then this results in a 50% reduction in the ductility usage available after irradiation ($\Delta U_{d\text{-}post}$). This is captured in the IAPs definition of the exhaustion of ductility rule (equation 4 in the IAP [2]) as reiterated here:

$$U_{d\text{-}pre} + \Delta U_{d\text{-}post} < 1$$

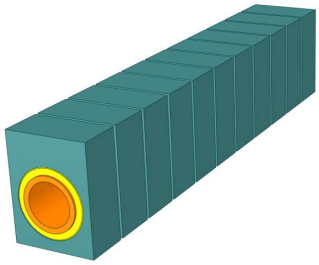

Figure 1Section from typical divertor plasma facing component comprising a series of individual tungsten armour blocks surrounding a CuCrZr cooling pipewith copper interlayer.

## 1.3 *Irradiated materials data.*

### 1.3.1 Source of irradiated materials data

Currently, irradiation effects are determined by measuring the response of materials irradiated in fission reactors. However, the fission and fusion neutron energy spectrum differ significantly as shown in Figure 2. Fusion spectrum have higher average neutron energies comprising fast neutrons (0.1 -14Mev) with a distinct 14MeV peak (from the D-T fusion reaction). Whereas fission test reactors provide either a mixed spectrum of both fast and thermal neutrons (eg RBT-6), or just fast neutrons but without the distinct 14MeV peak (eg Bor-60). This difference can cause significant effect in terms of the material's "irradiation" response.

Some of the many complications caused by testing with non-ideal fission spectrum are described by Fabritsiev [13]. For example, he states that "the high thermal neutron flux produces high concentrations of Ni and Zn transmutation products in copper … These solutes are known to strongly reduce the thermal conductivity"- Such complications necessitated Fabritsiev to overcome this effect by using cadmium cladding. In another case Fabritsiev noted that the threshold softening temperature for precipitation hardened copper alloys was found to be different for specimens irradiated in a mixed spectrum (SM-2) and a fast fission (BOR-60) reactor [3]. Perhaps most significantly, he noted that the absence of high neutron energy in fission reactors may lead to less helium gas production than would be expected in

fusion. This potentially leads to significant underestimate of embrittlement effects as discussed in section 2.3.2.1. It must be concluded therefore that current irradiated materials data needs to be treated with caution.

In this paper the level of irradiation is expressed in terms of the resulting displacements per atom (dpa) using a method that takes into account the effect of different energy spectrum. Most materials data referenced in this paper are from sources quoting dpa directly (rather than say fluence). However, it is noticeable that the method of calculating the dpa is rarely given.

Where only fluence values are given, an estimate of dpa is made using the FISPACT handbook [43] which gives estimated damage levels for all elements (H-Bi) for 3 fission reactor neutron-spectrum variants. The data from FISPACT allows approximate fluence-to-dpa conversion factors to be evaluated for each reactor type, as detailed in appendix 8.1.

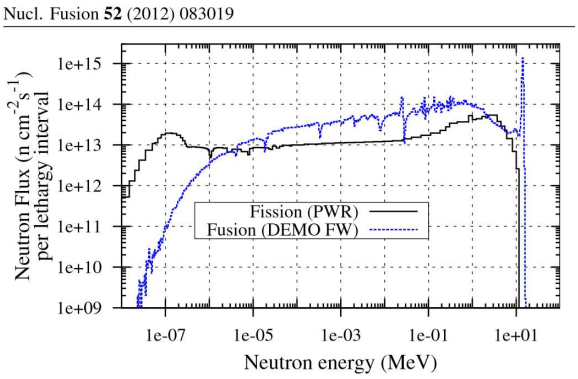


Figure 2 Comparison of neutron energy spectrum from Fission PWR and that expected in DEMO [53]

# 2 Irradiation effect on physical/mechanical material properties relevant IAP

## 2.1 *Property changes due to irradiation*

### 2.1.1 Thermal conductivity

Thermal conductivity is the principal thermal material properties influenced by irradiation and so has the greatest influence on the structural integrity of high heat flux components. Irradiation tends to reduce thermal conductivity and so results in increased temperatures which potentially reducing the materials strength, causes materials to be taken outside their known operating windows and increases the likelihood of tungsten recrystallization.

#### 2.1.1.1 CuCrZr And Copper thermal conductivity

Data on irradiated thermal conductivity for Copper and CuCrZr is taken from Fabritsiev [24] and the ITER MPH[28]. A number of competing effects have been noted, making the definition of a precise effect in the anticipated conditions in DEMO problematic.

For pure copper, Fabritsiev [13] noted the neutron spectrum of the irradiation source reactor, in terms of the thermal/fast neutron balance, affected test results. Fabritsiev measured resistivity changes to determine irradiation effects on thermal conductivity. These changes were split into those due to thermal neutron transmutation ($\rho_{tr}$) and those due to "radiation" defect component ($\rho_{rd}$). The latter achieved a saturation value of ~1 nΩm (i.e ~6% deviation from the unirradiated value) at 80°C (Figure 3) but that this decreases with irradiation temperature. Results suggest a negative effect at temperatures at T>250°C (Figure 4).

However, the ITER MPH incorporates the additional contributing effect of swelling (assuming that this was not included in the Fabritsiev measurements). It is noted that "the combined effect, based on the contributions of the solid transmutation, displacement damage (mainly at temperatures less than 200°C) and possible swelling (in the temperature range 250 - 450°C) will be no larger than 15-20% at the ITER lifetime fluence goal of 5 dpa". This is illustrated in Figure 5. However, the 1%/dpa contribution from swelling seems inconsistent with the existing swelling data discussed below. If all three contributors are included for the DEMO conditions of circa 13dpa but with a modified swelling effect value at 0.5%/dpa (see below), it could be concluded that the combined effect would cause a change in thermal conductivity of approximately 20%.

For CuCrZr, ITER [28] (with reference to Fabritsiev [13]), notes the same contributors for thermal conductivity loss as those described above for copper (based on the same reference material) without a contribution from swelling (which for CuCrZr is negligible as discussed below) . It is concluded that "The combined effect, …. will be no larger than 10 - 15% at the ITER fluence goal of 5 dpa." .

Pending further definition of the precise spectrum expected in the divertor, in this paper we use a representative conservative value for thermal conductivity reduction due to irradiation. For copper this is 15% and for CuCrZr 10%, based on a displacement damage effect of ~ 6%; swelling effect of 5% (in copper) plus a very rough allowance for possible thermal neutron contribution. It is acknowledged that this far from precise. No attempt has been made to estimate temperature dependence give the lack of precision in available data.

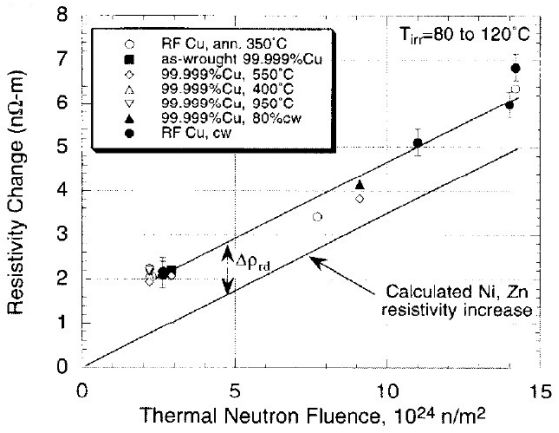


Figure 3 Fabritsiev [13] resistivity change in copper following irradiation in SM-2 reactor split into thermal neutron transmutation effect and saturation radiation damage effect $\rho_{rd}$

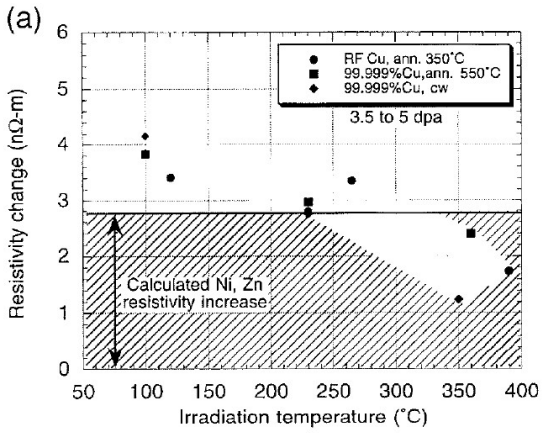


Figure 4 temperature dependence of resistivity change in copper due to irradiation in SM-2 mixed spectrum tractor [with calculated transmutation and radiation defect effect]

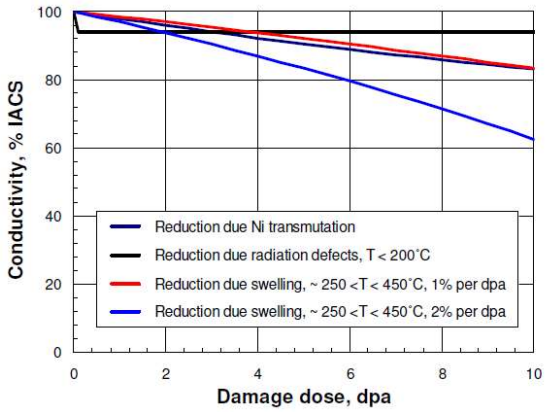


Figure 5 ITER MPH estimation of conductivity change due to transmutations radiation defects and swelling the same curves are provided for CuCrZr (but without swelling effect)

2.1.1.2 Tungsten thermal conductivity

Estimates of the change in thermal conductivity in tungsten due to irradiation have been gleaned from data on the associated changes in thermal diffusivity. Fujitsuka [29] made a study at low neutron fluences ($1{:}03e^{20}/3{:}37e^{19}$ thermal/fast respectively) estimated to be less than 0.1 dpa (using the method given in appendix 8.1). This caused a change in diffusivity of circa 15% at room temperature.

Studies at irradiation levels up to a quoted 5.6 dpa were carried out by Habainy [8], but in this case specimens were irradiated in ESS (European spallation source) i.e a combination of proton and spallation neutron irradiation. Habainy noted the difference caused by proton and neutron irradiation and it is assumed in this paper that the damage from these dissimilar effects are combined in the calculated dpa quoted.

Habainy found that 3.9 dpa irradiation caused an almost 50% reduction in thermal diffusivity at room temperature (Figure 6). This was identical to that at 5.9 dpa, suggesting a saturated level was achieved. Figure 6 shows also that the change in diffusivity reduces with temperature such that at the maximum (500 °C) temperature tested the change is circa 25%.

In order to estimate thermal conductivity-change from Habainy's diffusivity data, approximations have been made. Firstly, it is assumed that density (swelling) and heat capacity changes are a relatively insignificant factor in the observed diffusivity change and so conductivity change is approximately identical to diffusivity change. Secondly the data is extrapolated, with the observation that at temperatures > 1200 °C the change in diffusivity (and so conductivity) become negligible. The extrapolated estimate of conductivity values used in this study are shown in Figure 7.

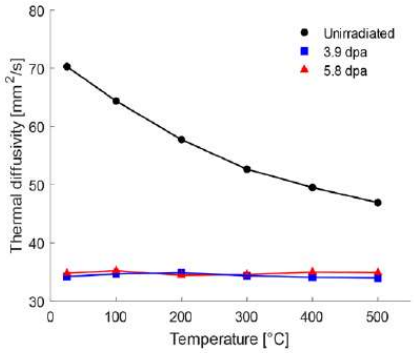


Figure 39 Thermal diffusivity of irradiated tungsten.

Figure 6 measured change in tungsten diffusivity as a result of irradiation in ESS (Habainy [8])

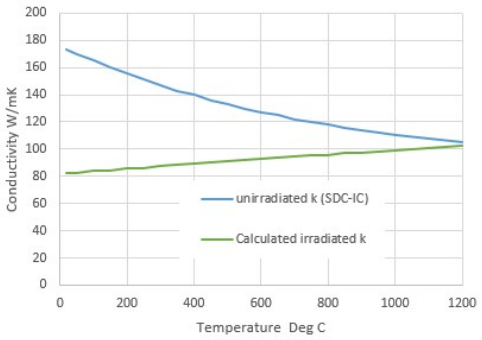


Figure 7 estimated change in tungsten thermal conductivity at dpa > 3.5 dpa based on the data from Habainy [2] using ESS radiation as shown in Figure 6

### 2.1.2 Density change (swelling)

#### 2.1.2.1 Copper swelling

Zinkle [18] studied the swelling of pure (low oxygen) copper under high levels of irradiation and in two samples measured 2.5 and 4.8% swelling at 16.9 dpa 375°C [in FFTF MPTOA 2B (fast neutrons)]. Zinkle points out the important contribution of even small amounts of helium generation (via fast neutron transmutation effects) in enhancing the stability of void nuclei. This is approximately in-line but slightly less the results of a previous study by Watanabe et al [30] (in their study of the effects of cold work) which gave swelling at circa 5% at 12.7 dpa in the annealed condition (FFTF MOTA at 696 793 and 873K). Watanabe also stated that swelling was assumed to be independent of temperature. For the purposes of the current paper a swelling value of 5% is used as representative of expected conditions. (There is insufficient data to assign a temperature dependence to this value)

#### 2.1.2.2 CuCrZr swelling

Singh [31] studied the swelling of both copper and CuCrZr under the effects of fast neutrons. Even though the tests were less than ideal because of poor temperature control (copper swelling varied from 2.85 to 10.72 at circa 30dpa) the results for CuCrZr swelling were low at less than 0.55%. This conclusion is also drawn by Zinkle [15] with reference to work of Garner [32]. For this reason, in this paper it is assumed that irradiation swelling in CuCrZr is negligible.

#### 2.1.2.3 Tungsten swelling

A comprehensive review of the effects of irradiation on tungsten is provided by Reith [19] who identified two key papers on swelling by Matolich [20] and Bykov[21]. The single crystal data from Bykov (1971) are summarised by Figure 8 which shows that under a fluence of 1.4e22 n/cm² density changes of 1.2% were recorded at 500°C reducing to ~0.15% at 2000°C. The reactor used for these tests is not specified so an estimated equivalent dpa value of 1.5 dpa is calculated using the approximate $0.8 \times 10^{22}$ n/cm²/dpa conversion factor described above. It is assumed that swelling is directly proportional to dpa so the above data equates to swelling values of 0.8%/dpa at 500°C and 0.1%/dpa at 2000°C)

The 1974 Matolich data, as shown in Figure 9, was gathered at higher irradiation levels (a quoted 9.5 dpa using the experimental breeder reactor EBR-II). This shows correspondingly higher levels of swelling but with more variability and a suggestion of an opposite temperature trend to that shown by Bykov. Most significantly, the data indicates a peak in swelling at 700-800°C (temperatures not included in the Bykov data) Here the swelling is ~1.6% (0.17%/dpa) which is approximately twice that suggested by Bykov.

For this paper primarily the data of Bykov is adopted. At the expected 4dpa damage level in tungsten (2 dpa/fpy), simulations use a swelling value of 3.2% at 500°C reducing linearly to 0.4% at 2000°C. However, it is acknowledged that the supporting data is far from satisfactory.

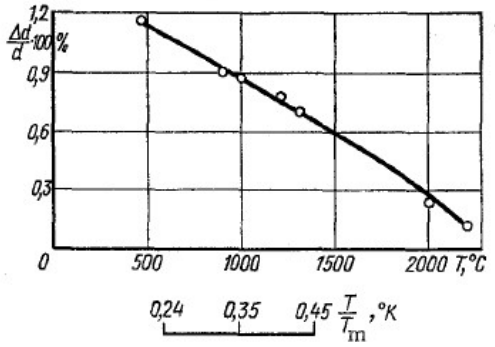


Figure 8 Tungsten swelling data from Bykov [21] Curve of "restoration of density" in isochronal annealing of tungsten single crystals, irradiated with a dose of $1.4 \times 10^{22}$ n/cm 2 at 0.20-0.21 $T_m$ estimated here to equate to 1.5dpa.

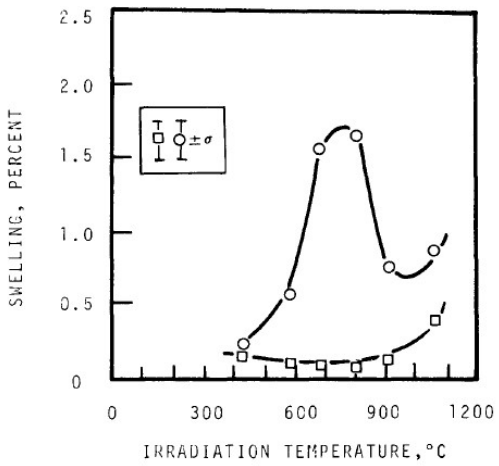


Figure 9 Tungsten swelling Matolich [20] for pure tungsten (o) and tungsten 25% rhenium (□) using EBR (fast neutrons 5.5 $\times 10^{22}$ n/cm² and stated 9.5dpa)

## 2.2 *Properties (yield & stress strain curves)*

A complication of the use of elasto-plastic (or inelastic) methods inherent to the IAP method is that the full true-stress true strain-curves are required to characterise the material. While there is a moderate amount of data on the change in yield strength of Cu/CuCrZr resulting from irradiation, the necessary data on the change in stress-strain curves is scarce. Moreover, trying to estimate irradiation effects across a range of sources is further complicated by the variety of heat/mechanical treatments used in standard materials/component manufacturing processes which potentially cause greater difference in mechanical properties then those caused by irradiation. Cold work of copper for example can increase the yield strength by a factor of 5 [52] and CuCrZr heart treatment and cold work variants influence yield strength by nearly a factor of 2 [36]. Unfortunately, many publications on the effect of irradiation on stress-strain characteristics provide little information on the base material condition, or if they do, then this may be significantly different from the ITER reference condition considered in the IAP (copper: Annealed w/o CW, CuCrZr Solutional annealed aged 2hr at 470°C "Treat B"). This must be considered when viewing the following assessment of the effects or irradiation on mechanical properties.

### 2.2.1 CuCrZr irradiated monotonic stress strain curves

Finici [16] published engineering stress-strain curves (Figure 10) showing that at 150 °C irradiation causes an increase in yield strength (of circa 25%) and an apparent post yield strain-softening characteristic. However, at 250°C the increase in yield strength is minimal and the post-yield characteristic has a level of strain-hardening similar to the unirradiated case. This suggest a "low temperature" embrittlement process occurs.

The illustrated levels of post-yield strain-softening shown in Figure 10, at 150°C appear to be significant. However, it has been demonstrated by Kamaya [28] that the apparent softening effect in test data such as this is due primarily to the combined effect of necking and the use of gauge length for strain measurement (rather than local true strain measurement).

To determine the true-stress-strain characteristics from the published irradiated materials test data (as shown in Figure 10 and the like) a methodology similar to that used by Kamaya has been used. The tests are simulated using a FE model (as detailed in Appendix section 8.2) and the material's true-stress strain curve determined by trial and error so that the models gauge-length strain-measurement matches the published test value. Results of the matched simulated 'engineering' curves are shown against the measured data in Figure 10. The derived true-stress strain data used to achieve these engineering curves is shown in Figure 11.

In the Finici reference unirradiated data, the yield stress for CuCrZr is approximately 400Mpa, which is approximately twice that of the reference IAP material. This discrepancy is due primarily to the material cold work manufacturing treatments used by Finici (annealed, 44% CW and aged 1Hr at 460°C). For the purposes of this paper the Finici data is used only to provide indicate relative effects, and the stress values used in the created true stress strain curves (unirradiated an irradiated) are halved to allow comparison with the IAP reference material condition stated above. It is suggested that potentially the hardening effects of irradiation could be more severe than Finici data suggests if the unirradiated condition had a lower yield strength.

The Finici data provides just two temperature conditions of 150°C and 250°C. To cover the expected temperature range of 20°C to 400°C, the expected trend at 200°C and 400°C is estimated by the following method: At 200°C the yield point and level of strain hardening is set to be linearly interpolated from the 150°C and 250°C condition. At 400°C the yields stress is extrapolated linearly from the 150°C and 250°C levels but the level of strain hardening is set to be equivalent to that at 250°C.

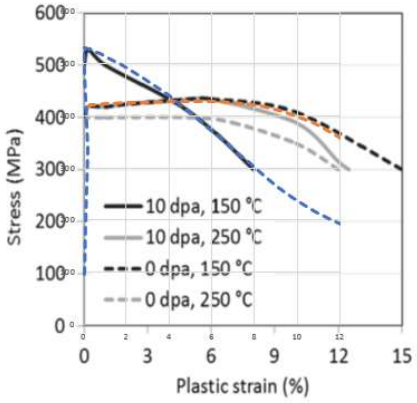


Figure 10 Comparison of Irradiated (in solid line; 10dpa Petten HFR) and unirradiated (dashed line) stress- strain curves for CuCrZr (annealed, 44% CW and aged 1Hr at 460°C) at 155 and 255°C [16]. Showing also comparison with simulated uniaxial test results (in colour)

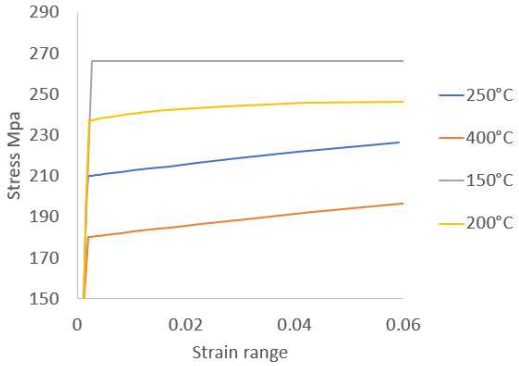


Figure 11 derived true stress strain curves for irradiated CuCrZr at 10dpa (derived by trial and error to achieve fit of simulated "engineering" stress strain data and Finici test data shown in Figure 10 with stress values halved)

2.2.2 Copper irradiated monotonic stress-strain curves

Stress-strain curves for irradiated pure copper are similarly as scarce as those for CuCrZr. For this paper the data provided by Fabritsiev [17] (Figure 12) and Zinkle [42] (Figure 13) is used. This suggests even greater (yield) strength increase from irradiation than in CuCrZr, but similar properties of "displayed" strain softening following yield.

The Fabritsiev/Zinkle data provides information at 80˚C and 200°C for irradiation levels of 0.08 and 13dpa resp. In this paper, aspects of the shape of curves at other temperatures and at higher levels of dpa have been inferred from published data on discrete measurements of yield strength and uniform elongation. The yield stress data from Li [23] for example Figure 14 shows that the hardening effect appears to saturate at about 0.1 dpa, so it is concluded that the Fabritsiev curve is approximately representative of higher irradiation levels. This appears to be confirmed by the curve from Zinkle at 13dpa (Figure 13).

To estimate the response of irradiated copper at other temperatures, the yield strength and uniform-elongation data from Zinkle [15] [44] has been used. The yield data (Figure 15) shows that at low temperatures the strength is dramatically increased by more than a factor of 5 – roughly in agreement with Fabritsiev [17] and Li[23] but with increasing temperatures this drops linearly, eventually approaching that of the unirradiated condition at 250°C.

The uniform elongation data from Zinkle (Figure 16) is used to estimate the post-yield characteristic of the irradiated stress-strain curve. Nonzero uniform elongation data gives an indication that strain hardening occurs. The data shows that at temperatures below 200°C, irradiated copper has no apparent strain hardening ability (as illustrated for example by Fabritsiev curve at 80°C), but above this temperature, hardening over a substantial amount of strain is achievable.

For the purposes of the IAP, it is initially postulated that at temperatures below 200°C, the shape of the irradiated copper stress-strain curve is the same as the irradiated curves shown by Fabritsiev in Figure 12, At temperature above 200°C, where copper shows reasonable levels of uniform elongation, stress strain curves are based on those of the unirradiated material in Figure 12. Nonetheless for all temperatures, the yield strength follows the temperatures dependence shown by Figure 15.

This postulated relationship needs to be confirmed because of an apparent inconsistency between the above uniform elongation data and the total elongation data presented by Fabritsiev discussed below in section 2.3.2.1.

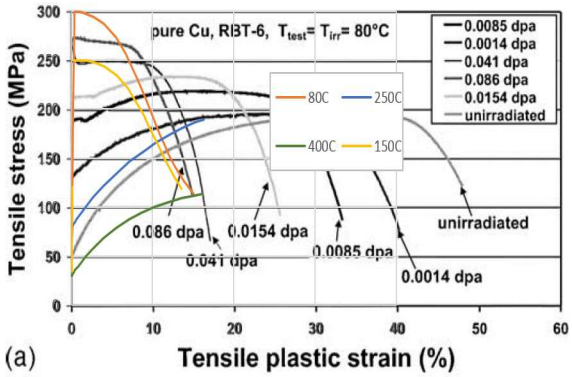


Figure 12 Effect of neutron irradiation to 0.0014–0.086 dpa on the engineering stress–strain curves of pure Cu **RBT-6** reactor $T_{test}$ =$T_{irr}$ = 80 °C. Fabritsiev [17] data in monochrome, with simulated tests data in colour.

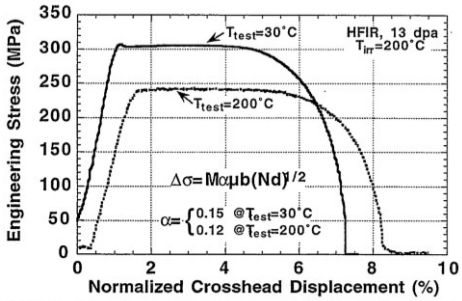


Fig. 2. Uniaxial load-elongation curves for pure copper irradiated to ~13 dpa at 200°C and tested at 30 and 200°C (specimens A6 and A8).

Figure 13 Stress strain curve of pure copper at 13dpa and 200°C (Zinkle and Gibson[42])

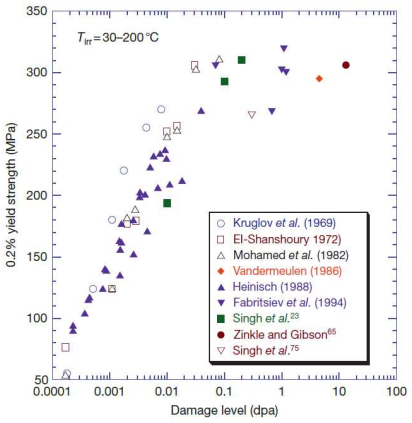


Figure 14 Saturation of hardening effect wrt dpa Radiation of copper from Li[23]

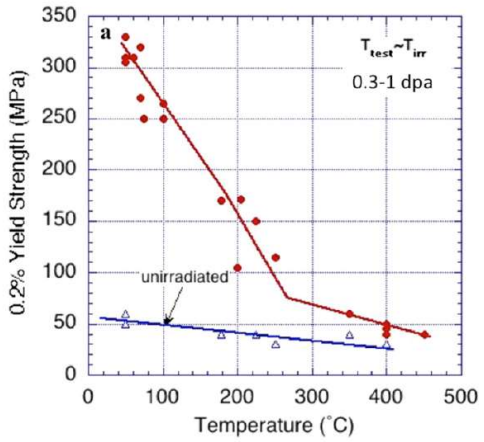


Figure 15 Effect of irradiation temperature on the yield strength of copper from Zinkle [9]

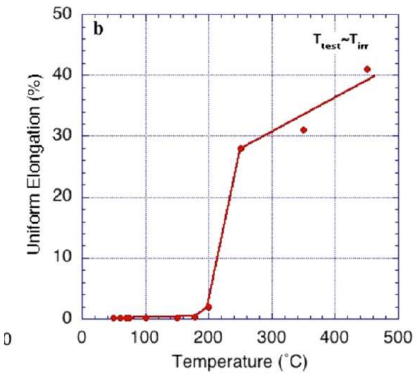


Figure 16 Effect of irradiation temperature on the uniform elongation of copper from Zinkle [15]

### 2.2.3 Cyclic stress strain curves Copper and CuCrZr

Two of the IAP assessment rules apply to cyclic load conditions (fatigue and ratcheting). Only one publication (by Singh [29]) was found showing the effects of irradiation on cyclic stress strain characteristics. Singh carried out tests on copper irradiated at 50°C to 0.5dpa (DR-3 reactor at Risø). The cyclic tests were performed after irradiation so do not entirely simulate the expected simultaneous irradiation and cyclic conditions, but the results are informative. The data (Figure 17 and Figure 18] suggests that at low strains irradiation hardening occurs. However, at higher strain level, with significant cyclic plasticity, any irradiation hardening effects are effectively erased, and the cyclic stress strain reverts to the unirradiated condition. It is assumed that under simultaneous irradiation and cycling, similar effects are observed.

No cyclic stress-strain data was found for CuCrZr. However, the data for dispersion strength copper (CuAl-25) shown in Figure 19 (Singh [35]) displays a similar removal of irradiation hardening at higher strains as that seen in pure copper. It is postulated that precipitation hardened CuCrZr will behave in a similar manner. For the IAP it is thus assumed the level of low-strain irradiation hardening in CuCrZr cyclic curves will be similar to that shown by the monotonic curves, while at high strain the curves revert to the unirradiated cyclic response.

Modelling the possible subtleties of cyclic behaviour suggested by the above, are beyond the scope of this paper. For example, low strain behaviour might depend significantly on the strain amplitude experienced in previous strain history. In this paper, variation in cyclic strain range is ignored. Furthermore, the dip in effective strength at intermediate strain range is also ignored. Hence for the IAP a rough simulation of the cyclic curve is created by using a simple bilinear characteristic as shown in Figure 20.

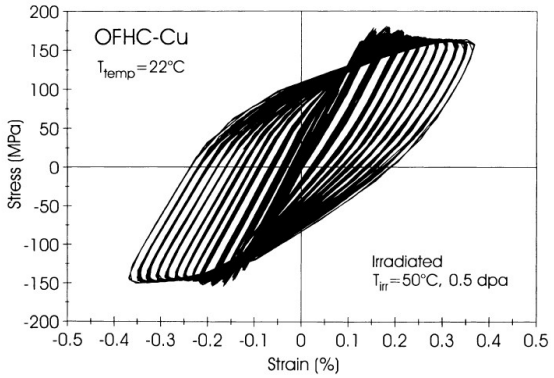


Figure 17 cyclic stress strain curves of irradiated copper at increasing levels of strain range (Data from Singh[29])

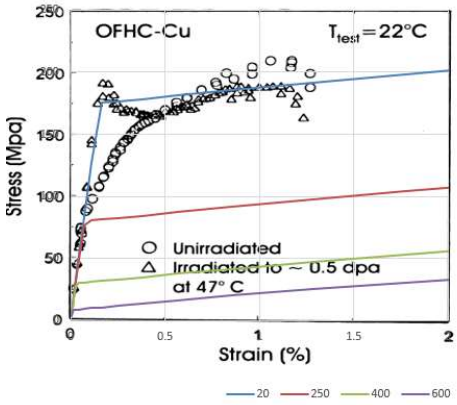


Figure 18 a summary of the irradiated copper cyclic stress strain data in comparison to the unirradiated response. (Data from Singh[29])

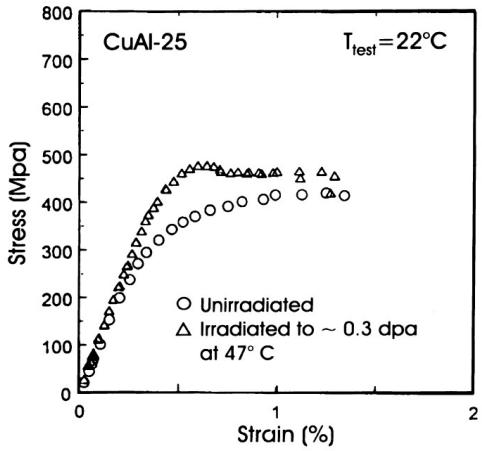


Figure 19 The cyclic stress strain response of dispersion strengthened copper from Zinkle [35]

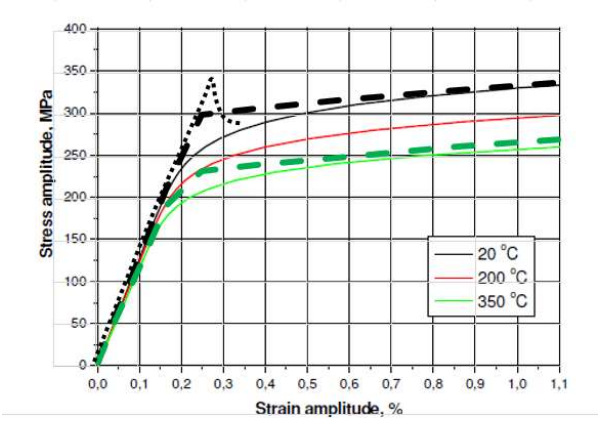


Figure 20 Postulated cyclic stress strain curve for irradiated CuCrZr by Chaboche simulation (solid lines = unirradiated condition (from [36]), short dash= estimated irradiated response, long dash= Chaboche model fit to estimated irradiated response for analysis.

## 2.3 *Damage limits (CuCrZr, Copper Tungsten)*

The following presents the material damage limit data that is relevant to three of the four principal ductile assessment rules (& damage mechanisms): true strain-at-rupture (exhaustion of ductility), fracture-toughness K1c (fast fracture), e-N data (fatigue). The fourth rule (ratcheting) does not have an explicit material limit [2].

Note : ITER SDC-IC App A [36] provides a range of (recommended) limit data for dpa levels up to 5 dpa (mostly from data to <3 dpa) but much of the underlying data are from internal unpublished reports so it is not always possible determine whether (or how) this data might be applicable to higher DEMO levels of dpa.

### 2.3.1 Irradiated CuCrZr limit data

#### 2.3.1.1 Rupture strain

In the absence of true-strain at rupture data for irradiated CuCrZr, a conservative estimate is derived from total elongation data provided by ITER [31] and the data from Fabritsiev [8]. The referenced underlying data from ITER is extensive but not published. It follows roughly the trend shown in the review by Zinkle [44]. All sets of data are for low dpa levels (< 3) and for the solution annealed and aged condition (ITER treatment "B").

The data sets are, to some extent, conflicting. The data from ITER (Figure 21) and Zinkle (Figure 23) suggest a strong trend with temperature. In contrast, the Fabritsiev data (Figure 22) suggest that for temperatures between 150 to 300°C (0.5<dpa<2.0) the total elongations are roughly scattered in a band between 10 and 20% without obvious temperature trend. It is notable that the Fabritsiev data suggests a much higher level of total elongation at 150°C than that indicated by ITER.

There is little data to suggest total elongation levels at the 13dpa DEMO level of irradiation. The Fabritsiev data shown in Figure 22 (at dpa<2.5) suggests an absence of obvious trend with increasing dpa. For the purposes of this paper this trend is assumed to extend to the DEMO condition, but clearly this need confirmation.

From the above it is proposed that for the purposes of initial DEMO irradiated PFC design assessments, the ITER data on total strain at rupture data should be used to estimate rupture strain. For the assessment shown later in this paper the best fit curve shown in Figure 21 is used.

Note: the ITER data suggest that below 150°C ductility is drastically reduced, but it is assumed that for DEMO, if these temperatures are to be imposed (e.g. for shutdown) a regeneration cycle will be performed to recover unirradiated properties.

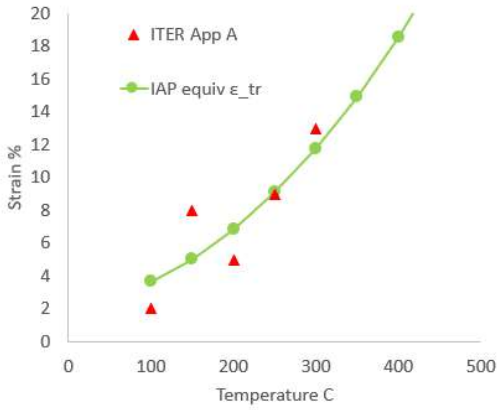


Figure 21 Minimum total strain at rupture data provided by ITER [36]for dpa in the range 0.3 to 5.0 (from test 0 2.5dpa) and proposed best fit curve for IAP exhaustion of ductility rule.

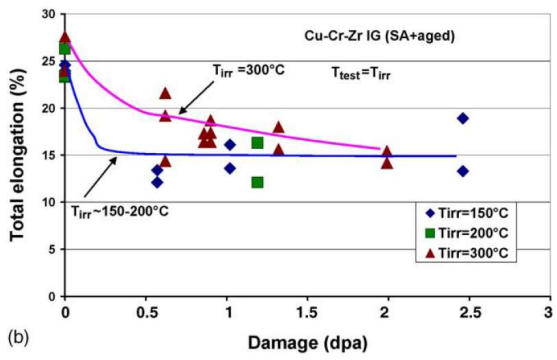


Figure 22 Total elongation data given by Fabritsiev [14] for irradiated CuCrZr at various dpa and $T_{iir}$=$T_{test}$ temperatures

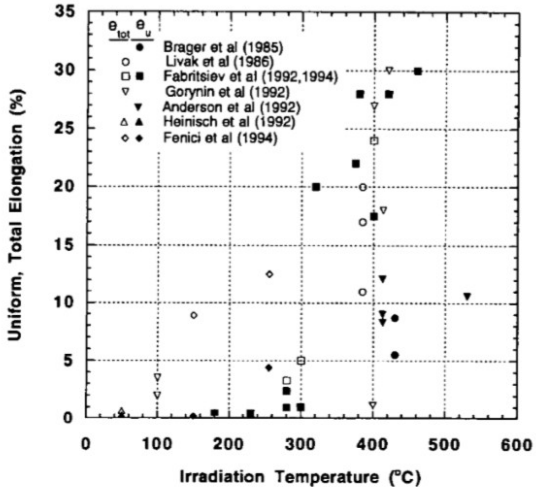


Figure 23 temperature dependence of total elongation for irradiated CuCrZr and ODS copper alloys from Zinkle [44] (the low elongation at 400C could not be confirmed from quoted Gorynin publication)

### 2.3.1.2 Fracture toughness

Published data on the fracture toughness of irradiated CuCrZr is only available at very low levels of dpa (to 0.3dpa at 0-500°C, or to 1 dpa at 80°C). The summary data taken from SDC-IC appendix A [36] (Figure 24) suggests a definite trend with temperature at 0.3 dpa but the values at higher temperature seem pessimistic with respect to the published data from Tahtinen et al [37] Figure 25.

The data shown in Figure 26 from Li[32] suggests there is no strong trend in fracture toughness with increasing dpa, but again only low-level dpa data is available. In the absence of better data this trend is assumed to extend to the 13dpa DEMO irradiation level.

Based on the above, a conservative extrapolation of the ITER data (as shown in Figure 27) is proposed as an estimate of toughness limit for DEMO PFC irradiated design assessment.

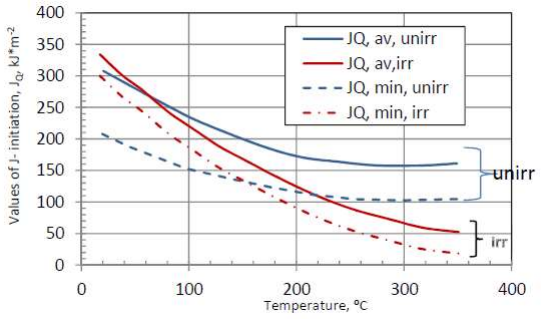


Figure 24 recommended Fracture toughnes data for unirradiated and irradiated solution annealed+aged CuCrZr from ITER SDC-IC App A [36]

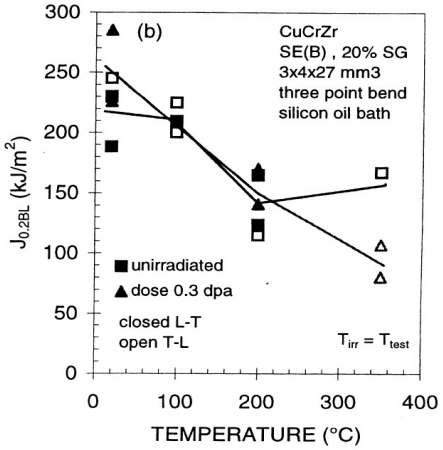


Figure 25 Fracture toughness data for irradiated CuCrZr from Tahtinen et al [37] various irradiation temperatures at 0.3dpa (DR-3 reactor -solution annealed and aged = ITER treat B)

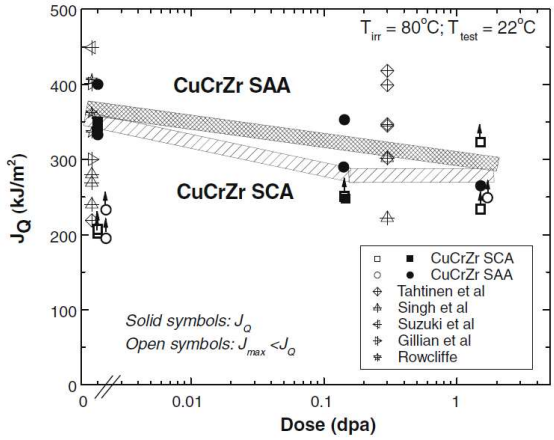


Figure 26 Fracture toughness of Irradiated CuCrZr at various dpa from Li M et al [38]

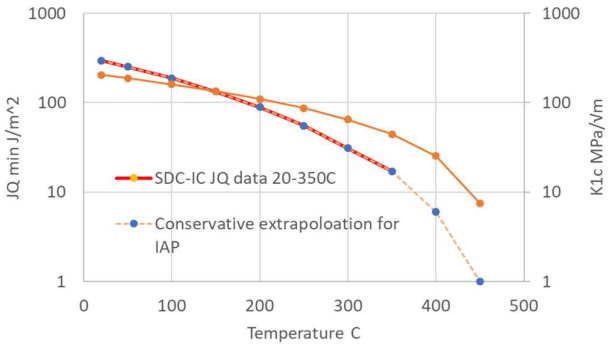


Figure 27 proposed fracture toughness characteristic for the IAP assessment of irradiated Solution annealed + aged CuCrZr.

### 2.3.1.3 CuCrZr Fatigue limit data

As above, published data on the fatigue strength of irradiated CuCrZr is only available at low dpa <= 0.3dpa Li Stubbins [39]. Observations of this data are summarised by the statements in ITER SDC-IC App A [36] that at 300°C, irradiation does not appear to have any significant effect on the number of cycles to failure. This seems consistent with observations from cyclic stress strain data described above that cyclic curves from irradiated material are similar to the unirradiated case (albeit at low dpa levels). Possibly there is also some correlation in fatigue and the observed independence of fracture toughness with dpa suggested above. In the absence of better data for the IAP the assumption is made that unirradiated fatigue data in CuCrZr retains its relevance at the higher DEMO dpa levels.

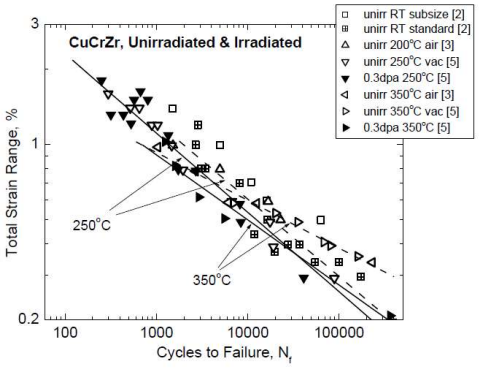


Figure 28 Effect of 0.3 dpa irradiation on the fatigue strength of CuCrZr at 230 and 350°C from Li Stubbins[39]

### 2.3.2 Irradiated Pure Copper Limit data

#### 2.3.2.1 Copper Rupture strain

Like CuCrZr, total strain at rupture is used as a conservative indicator of true strain at rupture for Copper. Much of the published data referenced by ITER [36] on irradiation effects on copper elongation are not only at low dose levels <0.5dpa but also at low temperature <=50°C.

However the publication by Zinkle and Gibson [42] shows a stress strain curve for pure copper (Figure 13 above) with irradiation to 13dpa at 200°C (Ttest=Tirr). Although this suggests a total ("crosshead%") elongation of just 8% is achieved, a steady strain softening is shown for elongations above 4% suggesting necking and potentially both high levels of ductility and high true strain at rupture.

In contrast, Fabritsiev [40] obtained elongation results (as shown Figure 29) for a wide range of test temperatures for copper irradiated at 335-345°C and an estimated dpa level of 2 (using the conversion factors described in Appendix section 7.1). This data exposed a mechanism he termed "340°C embrittlement", which results in almost a complete loss of total elongation at temperatures above 300°C. Fabritsiev attributed this "disastrous embrittlement" to an effective helium accumulation on the grain boundaries (due to entertainment) during a accumulating recrystallization under irradiation.

Given the very high levels of helium gas production expected in copper from Fusion neutron spectrum (FISPACT [43]), the Fabritsiev curve is deemed the more relevant limit for DEMO PFC assessment purposes.

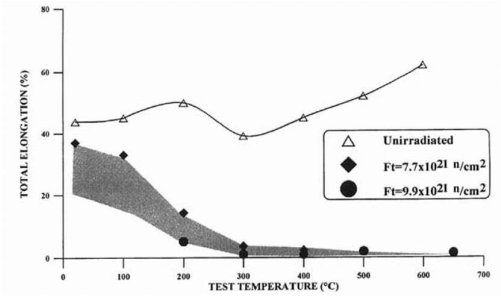


Figure 29 Total elongation of irradiated copper as measure by Fabritsiev [40] for a range of test temperatures at an estimated 2 dpa. (Bor-60 reactor)

#### 2.3.2.2 Pure copper fatigue

The closest relevant data on the effects of irradiation on the fatigue strength of copper is only available at very low irradiation doses as shown in Figure 30 (the quoted fluence 42 n/cm x $10^{18}$ is estimated to be equivalent to 0.01dpa). Also the data covers high cycle fatigue and at 50°C only.

In order to estimate low cycle fatigue strength at higher irradiation levels it would perhaps be tempting to use the same argument used for the CuCrZr. There it was observed that at higher strains the cyclic curves of the irradiated material reverts to that of the unirradiated material as discussed section 2.2.3, and so it was suggested that the low cycle fatigue strength of irradiated material may be similar to the unirradiated material. However, for copper this seems to be potentially at odds with observations of the "disastrous" helium embrittlement mechanism discussed above for temperatures >350°C. For this reason, it is concluded that no recommendation can be made for estimating the fatigue life of irradiated copper at these temperatures, especially as these are the

temperatures likely to be experienced in DEMO PFC interlayer. This is clearly is a major concern.

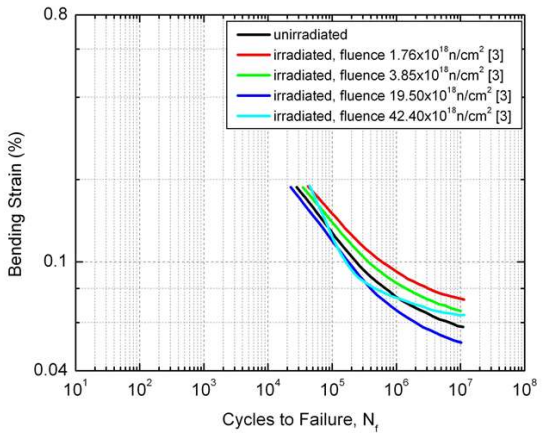


Figure 30 Fatigue data for irradiated pure copper from Strible [45]

### 2.3.3 Irradiated tungsten limit data

Currently the IAP assessment of the tungsten armour design is based on UTS and fatigue. However only data on the effects of irradiation on UTS could be found, so only a partial armour assessment is possible

Gorynin [46] observed a drastic loss in UTS to less than 100 MPa at irradiation temperatures from 300°C to 800°C as shown in Figure 32. (under a fluence $2e10^{22}$n/cm² estimated here to be ~2.5dpa). Higher strengths were reported by Haibainy [47](Figure 32) using spallation neutrons and proton source at dose levels 1.3 to 3.5 dpa. Data from Garrison [48] (replotted by Katoh [49]) Figure 34 suggest very fragile material properties in single crystal tungsten for dpa >1 reported as UTS~0 "handling failure". In contrast Gillemot [44] (as reproduced in [45]) found no significant effects of irradiation at 1.23 dpa (Figure 35).

Given that the majority of data suggests a significant drop in strength, for an initial guideline the assessment of DEMO irradiated PFC a UTS value of 100MPa is used.

Note, the absence of fatigue data prevents the application of the IAP deep cracking assessment methodology.

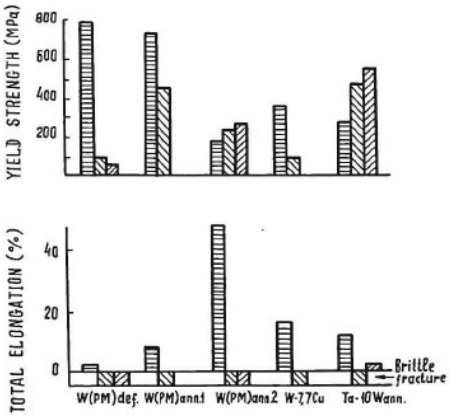


Figure 31 Gorynin [46] Strength data for irradiated tungsten.(irradiation was performed in the **SM-2** reactor (high thermal neutron flux) to doses $1x10^{21}$ n/cm² and $5x10^{21}$at $T_{iir}$ ~100°C and 300-500°C and in **BOR-60** reactor (Fast neutron reactor) to doses $8x10^{21}$ b/cm², $1.6x10^{21}$ n/cm² and $2e10^{22}$n/cm² at $T_{iir}$ 350,500 and 800°C)

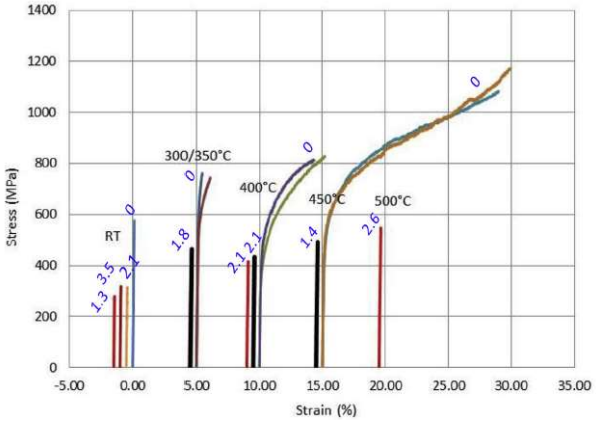


Figure 32 Tungsten strength data from Habainy [47], irradiated with high-energy protons and spallation neutrons in a target of the Swiss Spallation Neutron Source (SINQ) to doses in the range of 1.3-3.5 dpa, with 37-140 appm He, at temperatures between 75 and 110°C. During 3-point bending tests performed at temperatures up to 500°C

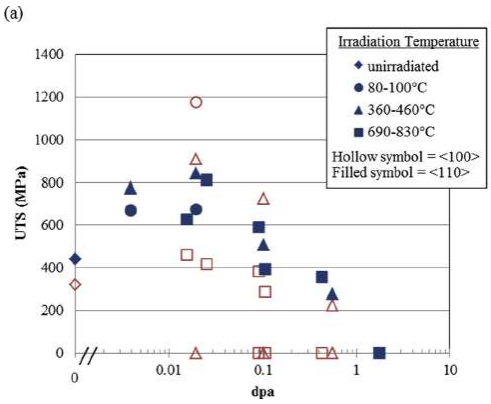


Figure 33 Garrison [48] single crystal (neutron irradiated in the mixed-spectrum High Flux isotope Reactor at the Oak Ridge National Laboratory at temperatures of 90-830 253°C to fast fluences of 0.01-$9x10^{25}$ n/m2 (E > 0.1 MeV).

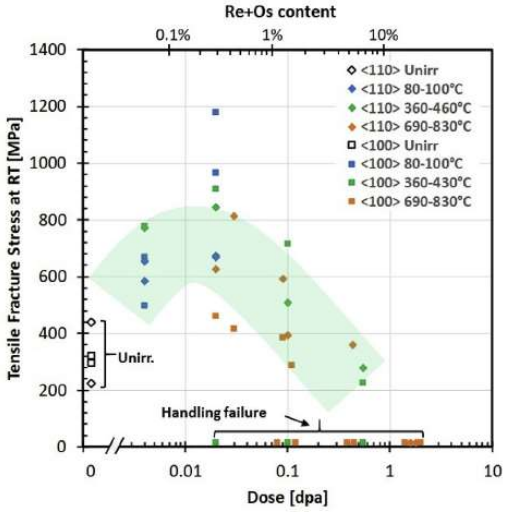


Figure 34 Katoh [49] (replotted from Garrison[48]). "Neutron irradiation in mixed spectrum reactors is an effective approach to investigate the synergistic effects of solid transmutations and atomic displacement damage in tungsten". Irradiation source: Oak Ridge as Garrison

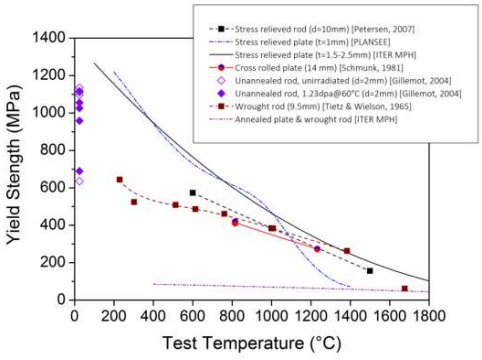


Figure 35 EuroFusion IDM 2MX5EF 2017 "MAT-1.2.1-T008-D001 – Material Handbook on tungsten (KIT)" with data from F. Gillemot, M. Horvath, G. Uri, A. Simonits, Neutron Irradiation Effects on Physical and Mechanical Properties of Tungsten, Final Report on TW!-TWP/TU3, HAS, Hungary, 2004.

### 2.4 *Summary of Irradiated materials data*

Table 1 provides an overall summary of the above irradiated materials data review and the recommended values extracted for use currently in the IAP pending further data. The table also includes an indication of the irradiation level of the source test data (in dpa) as an indicator of confidence that should applied to the values (relative to the DEMO dpa levels of 13dp for CuCrZr/copper and 4dpa tungsten)

Table 1 summary of irradiated data for use recommended for use in IAP pending further data

| | Material | Main source | dpa | Data |
|---|---|---|---|---|
| Conductivity | CuCrZr | Fabritsiev [13]/ITER | 3.5-5 | -10% |
| | Cu | Fabritsiev [13] | 3.5-5 | -15% |
| | W | Habainy[9] | 3.9-5.8 | Figure 7 |
| Swelling | CuCrZr | Singh[31] | 30 | ~0% |
| | Cu | Zinkle[18] | 16.9 | 5% |
| | W | Bykov[21] | 1.5 | 3.2%-0.4%(a) |
| Stress-strain (monotonic) | CuCrZr | Finici[16] | 10 | Figure 11 |
| | Cu | Fabritsiev[17] | 0.8/10(1) | Figure 12 |
| rupture strain | CuCrZr | ITER[36] | 2.5 | Figure 21 |
| | Cu | Fabritsiev[40] | | Figure 29 |
| fracture toughness | CuCrZr | ITER[36]/ Tahtinen[37] | 1 | Figure 26 |
| | Cu | - | - | - |
| Fatigue | CuCrZr | Li Stubbins [39] | 0.3 | Figure 28 |
| | Cu | - | - | - |
| | W | - | - | - |
| Strength | W | Gorynin[44] | 2.5 | 100MPa |

Key: "-" indicates no data

(a) 500°C-2000°C respectively

## 3 Example assessment of an irradiated PFC

To illustrate the implications of the above irradiated materials data on PFC performance, an example assessment of the benchmark monoblock divertor PFC in its simulated irradiated state is made. The assessment uses the IAP methodologies detailed in the part one paper but with the modified materials data. The results are compared with the assessment made of the component in its unirradiated condition presented in the Part1 paper [2].

### 3.2 *FE Model*

The example assessment uses the same ANSYS FE model used in the Part 1 paper but updated with the above devised irradiated materials data. The assessment includes a static thermal analysis and an elasto-plastic static structural analysis (the former to define the temperature distributions used as inputs for the latter). The defined requirement for this example component is 5000 "normal operation" pulses at 10MW/m² plasma heat load plus circa 300 slow transient events at 20MW/m² (an estimation of anticipated "normal" DEMO operations).

For both thermal and structural analysis, the monoblock was simulated by a quarter model with dimensions and typical mesh shown in Figure 5.

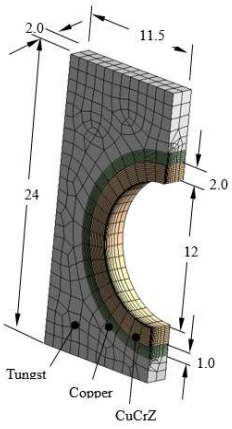


Figure 5 Quarter model geometry, dimensions and typical mesh using 23694 nodes.

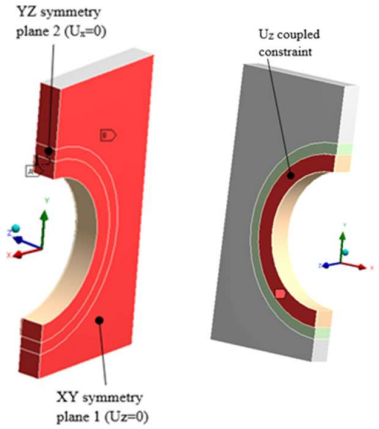


Figure 6 details of model constraints and pressure loading

### 3.2.1 Thermal model

As in the assessment of the unirradiated component in the part 1 paper, the thermal analysis was performed with 10MW/m$^2$ or 20MW/m$^2$ applied as an uniform heat load to the plasma facing surface (as illustrated in Figure 1). A convective cooling condition was applied to the pipe bore with a coolant heat transfer coefficient determined according to the Sieder Tate correlation extracted using the Thermprop program (as described in [2]) with water coolant flow of 16m/s at 5Mpa and 150°C.

### 3.2.2 Structural model and load cycles

Chaboche material models were used to define elastoplastic properties for the copper and CuCrZr (with constants listed in Appendix 8.3). Separate models were used for immediate failure assessment (ductility, fracture) and cyclic failure assessment (fatigue and ratcheting) by matching the respective monotonic or cyclic stress-strain curve estimates described above. For the purpose of this initial study, tungsten was defined as an elastic material data. Further studies are on-going of the effects of recrystallization (which would require elasto-plastic modelling of the recrystallized layer)

Structural model boundary conditions are shown in Figure 6. A couple constraint on the pipe end face was used to simulate the prevention of pipe bending (simulating the expected constraint of the monoblock support system).

For a complete assessment, load cases of shutdown (uniform 20°C), standby (uniform150°C), 10MW/m$^2$ and 20MW/m$^2$ would be considered, either singularly for monotonic rules or in combinations for cyclic failure assessment. In the following, for brevity, only the shutdown and 20MW/m$^2$ load case results are shown.

For the assessment of failure due to absolute stress/strain levels (i.e on the ductility and fracture rule) the heat load cycles are first simulated with unirradiated material properties followed by a number of cycles with properties modified to their irradiated values (using the ANSYS 'MPCHG' command) These cycles are preceded by manufacturing cycle to capture the expected stress and strain residuals from manufacturing (as described in the part 1 paper). By this method the accumulation of all strains during the life of the part are accounted for.

Swelling is simulated by adjustment of the materials coefficient of thermal expansion to add the required change in material volume (5% for copper or 3% for tungsten in the case studied). The swelling is assumed to be isotropic.

## 3.3 *Results*

The following describes the "low temperature" assessment result for exhaustion-of-ductility, fast-fracture, ratcheting and fatigue in the CuCrZr pipe; In the other materials only exhaustion-of-ductility of the copper interlayer and brittle fracture of the tungsten have been assessed due to lack of materials data.

### 3.3.1 Assessment of exhaustion of ductility in CuCrZr following irradiation to 13dpa

The immediate exhaustion of ductility rule ( reiterated below from section 2.1.2 of the IAP [2]) requires that the ductility usage $U_d$ is less than one. To account for changing ductility limits with irradiation, contributing usage fractions (=strain-used/strain-limit) are determined in the pre and post irradiation phases ($U_{d\text{-pre}}$, $\Delta U_{d\text{-post}}$).

$$U_{d\text{-pre}} + \Delta U_{d\text{-post}} < 1 \qquad \ldots. (4)$$

where the strain usage "$U_{d\text{-xxx}}$" is defined as follows:

$U_{d\text{-pre}} = (\varepsilon_{peq} + \varepsilon_{cf})/ (\gamma_d . \varepsilon_{Lpre})$

$U_{d\text{-post}} = \Delta\varepsilon_{peq\text{-irr}} / (\gamma_d . \varepsilon_{Lpost})$

and

$\Delta\varepsilon_{peq\text{-post}}$ = post irradiation incremental plastic strain

$\varepsilon_{cf}$ = equivalent manufacturing strain.

$\gamma_d$ = safety factor (0.5)

$\varepsilon_L$ = multiaxial strain limit (function of temperature T and fluence Φ).

In the example here, a postulated worst-case scenario is considered. In this scenario the target component sits in an area of the divertor not normally experiencing high heat loads, but later in life (following a significant period of irradiation) is subjected to a single intense load resulting from a misplaced target zone with loss of detachment – effectively a monotonic load of 20MW/m² in the irradiated state. Because the component has not experienced significant cyclic strains previously it will thus have the maximum hardening effect of irradiation.

Figure 38 shows the calculated resulting strain history at various key locations in the CuCrZr pipe for this scenario. (Note these are the mechanical strain components only and do not include swelling or thermal strains). The figure shows that the maximum strain increment occurs during the (isothermal) irradiation phase, and hence is due to irradiation swelling and hardening alone. The highest strain is experienced at location A at the strain concentration between adjacent armour blocks..

To make the assessment of these strain, the usage fractions, $U_{d\text{-}pre}$ and $U_{d\text{-}post}$ must be evaluated. However, the process can be simplified by noting that if the value of $U_{d\text{-}post}$ alone is greater than one then the rule is by definition failed (and so provides a simpler preliminary check).

A crude assessment of this usage is made by simply dividing an estimate of the post irradiation strain-range (from Figure 37) by ½ the limit-strain $\varepsilon_L$ from Figure 21. For location A, with the highest strains, the graphs suggest a usage value of roughly 0.44 (=.04/(0.5x.18)) (noting that the temperature of location A at 20MW/m² is circa 450°C). This estimate suggests the rule might be passed.

However, the full specification of the rule requires that strain range is evaluated accurately (using tensor components) and that multiaxial stress effects must be included in the limit-strain value (according to the IAP expression taken from ASME shown below). For this reason, a script is used to produce a contour plot of strain-range usage throughout the CuCrZr component taking into account local variation in temperature (and so ductility) and local value of triaxial stress (and so limit adjustment). This contour plot (Figure 38) reveals for example that significant usage occurs at location B, primarily because there is significant triaxial stress plus low temperatures at this location (~150°C- even under plasma heat load) leading to low rupture strain.

$$\varepsilon_L(T,\emptyset) = \varepsilon_{LU}(T,\emptyset) * Ktf\ (T) \qquad \ldots. (2)$$

$$Ktf(T,\sigma) = exp\left(-\left(\frac{\alpha_{SL}}{1+m}\right)\left(\left\{\frac{\sigma_1+\sigma_2+\sigma_3}{3\sigma_{eq}}\right\}-\frac{1}{3}\right)\right) \qquad \ldots. (3)$$

Finally, to fulfil the rule requirements it is necessary to consider all possible combinations of the load cycle start/finish points to expose the worst-case condition. A summary of the key results for the given scenario is given in Table 2 for cycle start /end points, with the key contributors to the final usage value listed. The highest usage value of 3.88 is found at location B for the full load cycle from the unirradiated condition at 150°C (normal op but no heat load) to the full irradiated condition with a single 20MW/m² heat load. However, it should be noted that most of this usage occurs during the process of (isothermal) irradiation without heating, where the usage is 3.44 (as shown above).

As a caveat, it should be noted that in practice the limit strain reduces progressively during irradiation so the use of the final limit strain in the above evaluation results in a conservative value of usage. A more precise value of usage would be achieved by a time integral evaluation based on time dependant irradiation data if this was available.

The above result shows a failure of the exhaustion of ductility design rule, indicating a potential for cracks to be initiated in the pipe wall leading to premature failure or leaks.

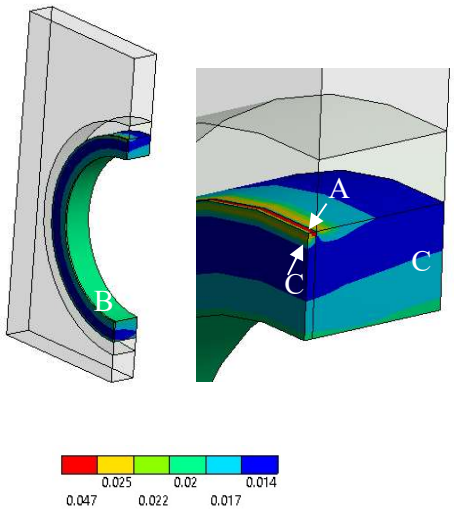


Figure 36 Calculated true strain in the CuCrZr pipe at 20MW/m² including the simulation effects that might be expected with 6dpa of irradiation (swelling and hardening)

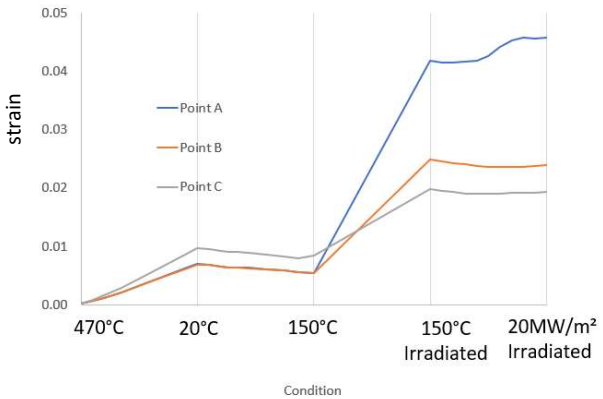


Figure 37 Strain history at locations A,B and C of the strains shown in Figure 36 showing that predominant strain increment occurs during the process of irradiation swelling

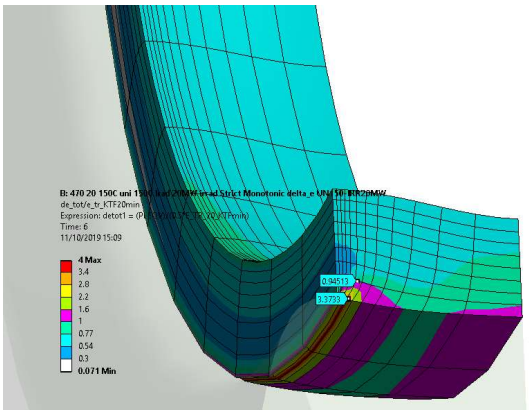


Figure 38 Ductility usage at location B resulting from incremental strains in the cycle step from the unirradiated condition at 150°C to a 20MW/m² heat condition plus the expected consequence of irradiation at 13dpa.

Table 2 Ductility usage fractions (and contributing factors) experienced at three key locations in the CuCrZr pipe and three cycle start-end points during/following plus the expected consequence of irradiation to 13dpa.

| | 150UN - 20MW/m² IRR | 150°C(IRR) - 20MW/m°(IRR) | 150°C(IRR) - 150°C (IRR) |
|---|---|---|---|
| location | B | C | B |
| Strain Δe | 0.016 | 0.010 | 0.015 |
| Δe % | 1.57 | 1.01 | 1.52 |
| k_tr | 0.16 | 1.00 | 0.18 |
| e_tr | 5.00 | 5.00 | 5.00 |
| Limit condition | at 20 | at 150C | at 150 (IRR) |
| k_tr*e_tr | 0.82 | 5.00 | 0.88 |
| Usage : Δe /(0.5 * K_tr * e_tr) | 3.81 | 0.40 | 3.45 |

### 3.3.2 Assessement of irradiated CuCrZr fast fracture (to 13dpa).

The Fast fracture rule aims to expose any potential for immediate fracture initiated by flaws already present in as-supplied materials (below by NDT threshold). In the IAP an analytic expression is used to determine what stress intensity $K_1$ would be created if a 0.2mm flaw existed anywhere in the local stress field. This must be shown to be less than the local (temperature dependant) value of critical stress intensity $K_{1c}$. This is achieved by plotting the usage fraction ( $=K_1/(\gamma_{K1}K_{1c})$ which must be less than 1 in order to meet the criterion:

$$K_1 < \gamma_{K1} K_c(T, \emptyset)$$

Figure 39. shows the fracture toughness usage fraction for the irradiated case at standby and at 20MW/m². In both cases the usage is less than 1, indicating that fast fracture is not deemed a risk.

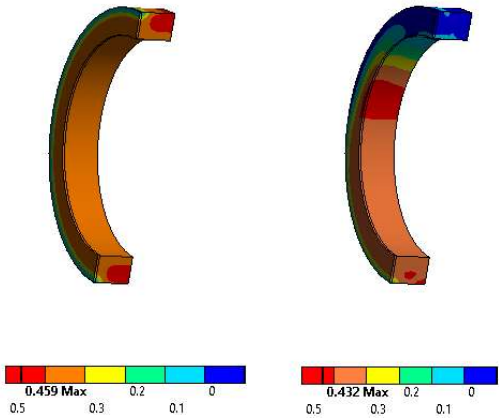


Figure 39 Fracture toughness usage in CuCrZr pipe at standby after irradiation (left) and with a subsequent single monotonic load of 20MW/m² (right)

### 3.3.3 Assessment of CuCrZr ratcheting

No significant deviation in ratcheting behaviour was found from that observed in the unirradiated condition as described in the part 1 paper [2]. As observed in the unirradiated case, the thermal gradient in the wall of the CuCrZr pipe is too insignificant to create conditions likely to cause ratcheting on a global scale (and the observed change in material thermal conductivity are far to slight to influence this result). Local ratcheting observed in the unirradiated condition was slightly less prominent in the irradiated condition, but as previously discussed conclusions about local ratcheting require significant further validation studies before they can be included in the assessment results with confidence.

### 3.3.4 Assessment of irradiated CuCrZr fatigue at13dpa

Figure 40 shows the calculated strain range in the CuCrZr pipe after irradiation (~13pda) for the cycle from 150°C to 10MW/m². As in the monotonic loading case, strain is concentrated in the gap between armour blocks, with maximum strain range of .45%. This is only a moderate increase in strain-range from the unirradiated condition (0.4%) considered in the IAP part 1 paper, but this results in a design fatigue life of only 1915 Cycles (compared with the nominal spec of 5000Cycles [(1)]).

The fatigue usage fractions for two of the highest load cycles are summarised in Table 3. This shows that any one of these load cases results in a design rule failure (i.e. usage >1). The total usage exceeds 5. This compares with the usage for unirradiated condition of 3.6.

(1) In practice this result is conservative since some of the fatigue usage occurs in an unirradiated case. It may be assumed actual usage lies within the range of 3.6 to 5.

Note the model simulates the ideal of a PFC fully constrained to prevent pipe bending (giving the desired constraint of the armour plasma facing surface position). Some relaxation of this constraint due perhaps to manufacturing tolerance/clearance in the fixing system may reduce strains)

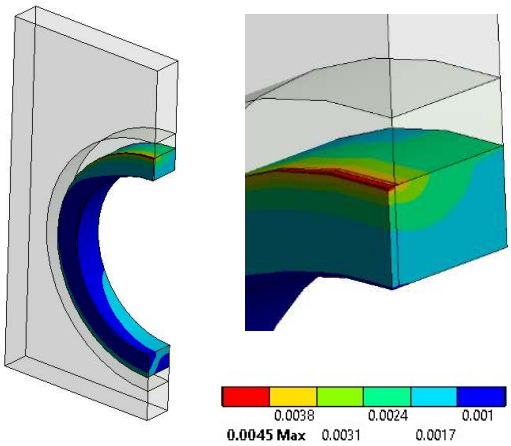


Figure 40 calculated intensity of strain range after irradiation, cycling from standby (150 °C) to 10 MW/m² heat load, with a maximum strain range of 0.45%.

Table 3 fatigue usage fraction for irradiated (~6dpa) CuCrZr for the two

| case | A | D |
|---|---|---|
| From | 150°C | 150°C |
| To | 10MW/m² | 20MW/m2 |
| Δε% | 0.45 | 0.99 |
| N | 1915 | 118 |
| Nspec | 5000 | 300 |
| Vi | 2.54 | 2.61 |
| ΣVi | 5.16 | |

### 3.3.5 Assessment of Copper exhaustion of ductility at 13dpa

The assessment of strain in the copper is made with the modified interlayer design used in the assessment of the unirradiated component [2]. Here the profile of the free surface of the copper interlayer is given a scalloped design (as illustrated in Figure 41) to remove the strain discontinuity at the dissimilar material interface between tungsten and copper (inherent in the conventional design).

Figure 42 shows the increment in strain in the step from the standby (uniform 150C) condition unirradiated to an irradiated condition with 20MW/m². In this case the 5% strain alone is sufficient to show that the material limit of <1-2% is failed. Effects of triaxiality further aggravate the conditions leading to an extremely high usage fraction >50. The result suggests that the interlayer would rapidly acquire cracks/defects following irradiation with the potential for an early failure of the interlayer which in turn would lead to overheating and potential failure of the Armour.

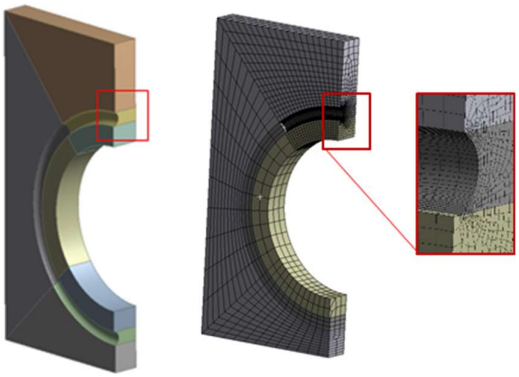

Figure 41 Modified interlayer design with scalloped copper surface to remove dissimilar material joint strain discontinuity (and model implementation used to achieve viable mesh and run times)

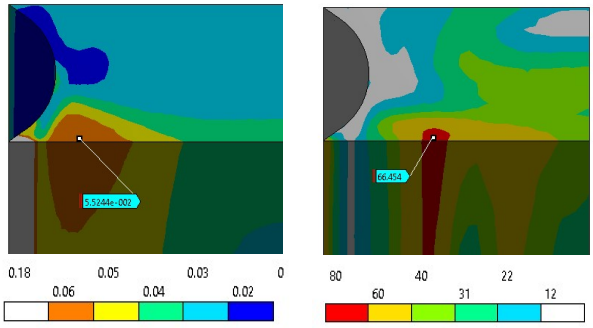


Figure 42 Strain increment in step from the unirradiated condition at 150C to irradiated condition at 20MW/m² heat load (left) and the resulting ductility usage factor (right)

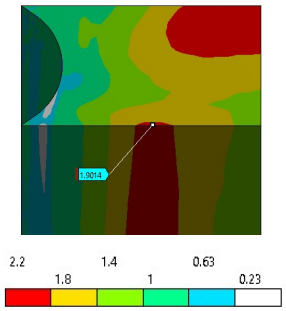


Figure 44 Strain increment from the unirradiated condition at 150C to 20MW/m² irradiated condition (left) and the resulting ductility usage factor (right)

### 3.3.6 Assessment of irradiated tungsten (4dpa)

Figure 43 shows that high levels of principal stress are created on the internal diameter of the tungsten during slow transient events with stress level of 661MPa. Results (not shown) demonstrated that these were tensile hoop stress. They should be compared with expected tensile strength of ~100MPa (from Figure 31) indicating a strength usage fraction >5.

The results suggest cracks are likely to occur on the bore of the armour following irradiation potentially leading to through cracks, which when combined with brittle failure of the interlayer (as discussed above) may result in separation of segments of armour from the pipe, and so total part failure.

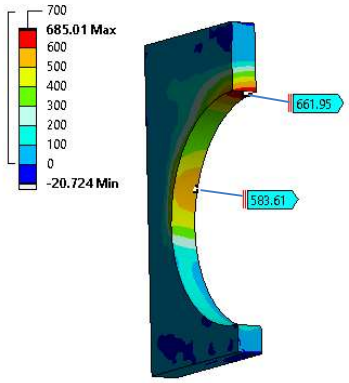


Figure 43 Maximum principal stress in tungsten at 20MW/m² (equates to a strength usage >5)

### 3.4 *Summary of irradiated vs unirradiated results*

Table 4 shows a summary of the IAP structural integrity assessment of the irradiated ITER-like component in the form of usage fractions (where a value greater than 1 indicates an assessment failure). Values are compared to those of the unirradiated assessment [2]. The gaps in the table indicate a lack of materials data.

Clearly the lack of ductility in the copper and strength (UTS) of the tungsten are the major concerns. Nonetheless the ductility and fatigue of the CuCrZr are also well above the "design" allowable indicating severe risk of at least crack initiation if not failure. Only fast fracture meets the required criterion.

It is reiterated that these results are only an estimate based on the materials data extrapolations described above.

Table 4 Summary of damage mechanism usage fractions in the irradiated condition (compared with unirradiated condition in parenthesis). Usage >1 indicates a design rule failure (-- indicates No data)

| | **CuCrZr** | Copper | Tungsten |
|---|---|---|---|
| Ductility | 3.81 (0.048) | >20(0.29) | N/A |
| Fracture UTS | 0.45(0.65) | -- | >5 (1.49) |
| Global ratcheting | (a) | (a) | N/A |
| Fatigue | 5.16 (3.63) | -- | -- |

(a) Global ratcheting was not observed

## 4 Summary and Conclusions

This paper is the second part of a 3-part paper describing the inelastic analysis procedure (IAP): a procedure created by EuroFusion's WPDIV group to give guidance for the structural integrity assessment of divertor plasma facing components (PFCs). Typically these components comprise tungsten armour attached to a CuCrZr cooling pipe via a copper interlayer. This part II paper deals with the assessment of irradiated PFCs (and associated analysis/assessment methodologies).

To make such assessments possible, irradiated materials data has been reviewed and estimates made of the relevant properties and limit-data at the expected DEMO dpa levels (13dpa Cu/CuCrZr, 4dp W). In many cases the irradiation level used in the materials test is very low and extensive extrapolation has been required. The key findings of the review and estimation exercise are as follows:

Property changes:

1. Thermal conductivity changes: -15% copper -10% CuCrZr, -70% to 0% for tungsten at temperatures from 500°C to 1200°C resp.
2. Swelling of 5% in copper 3% to -0.16% (500°C to 1200°C) in tungsten, negligible in CuCrZr
3. Significant modification of monotonic stress strain curve characterised for example by a potential factor of 5 increase in yield strength for copper with complete loss of strain hardening at T> 250°C. Cyclic curves are almost unchanged (Note the full stress strain curve is required in an IAP assessment)

Limit data:

1. Copper suffers a drastic helium embrittlement resulting in a rupture strain < 1% at T >350°C
2. Tungsten (cold rolled) suffers a drastic loss of strength from > 900MPa to circa 100MPa.
3. CuCrZr loses ductility at T < 150°C, but toughness appears to be less affected.

Main limitations in the current data:

1. Low or very low dose levels, compared with that expected in DEMO (much test data is for dpa<2 ; fatigue <0.3)
2. Data for the major areas of concern in tungsten (loss of strength), and copper (helium embrittlement) rely on a single source.

The above data has been used to demonstrate the application of the IAP in the structural integrity assessment of an ITER-like component irradiated to the expected DEMO irradiation levels. The additional irradiation specific methodologies introduced in this paper (over these detailed in part1 [2]) include the simulation of material property change (from unirradiated to irradiated state) so that strains at all stages of life are accumulated. Usage fractions for the pre and post irradiation are also used so that changes in both strain and strain limit before/after irradiation can be accounted for.

Beyond demonstration of the IAP process, the example analysis has also identified key areas of concern in the irradiated response of a typical DEMO PFC concept design (based on the ITER-like monoblock). These include:

1. Fracture of the copper interlayer, potentially causing thermal isolation of the tungsten from the heat sink leading to overheating and early failure.
2. Cracking on the ID of the tungsten armour which, when combined with the copper failure, potentially causes complete armour separation.

3. High cyclic strain on the surface of CuCrZr pipe in the gap between monoblocks leading to early fatigue cracks and potential coolant leaks.
4. A potential for local strain ratcheting in the CuCrZr in the gap between armour blocks (however this may be indistinguishable from fatigue failure)

Note: Fast fracture and global ratcheting of the CuCrZr pipe is not a concern.

The example illustrates that the demonstration of the structural integrity of a PFC in its irradiated condition is a far more demanding test of a design capability than that in its unirradiated state. Hence it is the irradiated condition that should be the focus of future design assessments.

By illustrating how and where irradiated materials data is used in PFC structural integrity assessments, the paper can be used as an aid in defining the requirements list for the irradiated materials test data necessary for future PFC design qualification.

# 5 Recommendations

1. Place the irradiated structural integrity assessment as a priority in PFC design studies
2. Obtain confirmation of irradiated tungsten strength loss and copper helium embrittlement
3. Investigate CuCrZr susceptibility to embrittlement at fusion relevant helium appm.
4. Replace copper with soft copper alloy alternative (e.g. overaged CuCrZr) for interlayer materials.
5. Perform design studies to significantly reduce stress in the tungsten (while retaining the monoblock designs armour retention functionality).
6. Extend Cu/CuCrZr fatigue data to representative irradiation levels.
7. Gather fatigue data for irradiated tungsten.
8. Gather cyclic stress strain data for irradiated PFC materials.

# 6 Acknowledgements

This work has been carried out within the framework of the EUROfusion Consortium and has received funding from the Euratom research and training programme 2014-2018 and 2019-2020 under grant agreement No 633053, and from the RCUK Energy Programme [grant number EP/T012250/1]. To obtain further information on the data and models underlying this paper please contact PublicationsManager@ccfe.ac.uk. The views and opinions expressed herein do not necessarily reflect those of the European Commission.

Acknowledgements to Lee Packer and Mark Gilbert for their advice on reactor neutron spectrum and fluence to dpa conversion factors

# 7 References

[1] T. Hiraia et al, Test Design optimization of the ITER tungsten divertor vertical targets Fus. Eng. Des. 127 (2018) 66-72.

[2] Fursdon M, You J-H, Li M, Towards reliable design-by-analysis for divertor plasma facing components –Guidelines for inelastic assessment (part 1: Unirradiated). Fusion Engineering and Design 147 (2019) 111234.

[3] You J-H et al, European DEMO divertor target: Operational requirements and material-design interface, Nuclear Materials and Energy 9 (2016) 171–176

[4] Fursdon M, You J-H, Li M, A hybrid analysis procedure enabling elastic design rule assessment of monoblock-type divertor components, Fusion Engineering and Design 135 (2018) 154–164

[5] M. Li, J.-H You, Interpretation of the deep cracking phenomenon of tungsten monoblock targets observed in high-heat-flux fatigue tests at 20 MW/m2, Fus. Eng. Des. 101 (2015) 1–8

[6] M. Miskiewicz, J.-H. You, Impact of plastic softening of over-aged CuCrZr alloy heat sink tube on the structural reliability of a plasma-facing component, Fus. Eng.Des. 83 (2008) 66–71.

[7] Gorynin I.V. Effects of neutron irradiation on properties of refractory alloys, Journal of Nuclear Materials 191-194 (1992),

[8] Habainy J. Characterisation of mechanical and thermal properties of tungsten for high power spallation target applications. PhD Thesis Lund University 2018.

[9] Habainy J et al. Mechanical properties of tungsten irradiated with high-energy protons and spallation neutrons. Journal of Nuclear Materials 514 (2019) 189-195

[10] Garrison LM, Katoh Y. et al. Mechanical properties of single-crystal tungsten irradiated in a mixed spectrum fission reactor Journal of Nuclear Materials 518 (2019) 208-225

[11] Y. Katoh Snead LL Garrison LM et al. Response of unalloyed tungsten to mixed spectrum neutrons. Journal of Nuclear Materials 520 (2019) 193-207

[12] J.H. You et al. European DEMO divertor target: Operational requirements and material-design interface. Nuclear Materials and Energy 9 (2016) 171–176

[13] Fabritsiev S.A. et al. “The effect of neutron spectrum on the mechanical and physical properties of pure copper and copper alloys” Journal of Nuclrnr Materials 233-237 (1996) 5266533

[14] Fabrisiev SA and Pokrovsky AS., Effect of high doses of neutron irradiation on physico-mechanical properties of copper alloys for ITER applications Fusion Engineering and Design 73 (2005) 19–34

[15] Zinkle SJ Applicability of copper alloys for DEMO high heat flux components Phys. Scr. T167 (2016) 014004 (10pp)

[16] P. Fenici, D.J. Boerman, G.P. Tartaglia a, J.D. Elen b. ‘Effect of fast-neutron irradiation on tensile properties of precipitation-hardened Cu-Cr-Zr alloy” Journal of Nuclear Materials 212-215 (1994) 399-403

[17] S.A. Fabritsiev et al. ‘Effect of the irradiation–annealing–irradiation cycle on the mechanical properties of pure copper

and copper alloy" Journal of Nuclear Materials 324 (2004) 23–32
[18] Zinkle Effect of initial oxygen content on the void swelling behavior of fast neutron irradiated copper Journal of Nuclear Materials 329–333 (2004) 938–941
[19] Reith M et al., Behavior of tungsten under irradiation and plasma interaction, Journal of Nuclear Materials 519 (2019) 334-368
[20] J. Matolich, H. Nahm, J. Moteff, "Swelling In Neutron Irradiated Tungsten And Tungsten-25 Percent Rhenium", https://doi.org/10.1016/0036-9748(74)90304-4. Scripta Metallurgica Vol. 8, pp. 837-842, 1974
[21] Bykov Change in density of single crustal tungsten during neutron irradiation. V.N. Bykov, G.A. Birzhevoi, M.I. Zakharova, Sov. At. Energy 32 (1972) 365-366, https://doi.org/10.1007/BF01116968
[22] You et al, Progress in the initial design activities for the European DEMO divertor: Subproject "Cassette". Fusion Engineering and Design 124 (2017) 364–370
[23] Li M. Zinkle S J., Physical and Mechanical Properties of Copper and Copper Alloys, Comprehensive Nuclear Materials (2012), vol. 4, pp. 667-690
[24] S.A. Fabritsiev a,*, A.S. Pokrovsky The effect of neutron irradiation on the electrical resistivity of high-strength copper alloys Journal of Nuclear Materials 249 (1997) 239-249
[25] B.N. Singh, J.F. Stubbins, P. Toft. The influence of neutron irradiation on the fatigue performance of OFHC copper and a dispersion strengthened copper alloy Journal of Nuclear Materials 275 (1999) 125±137
[26] M.R. Gilbert An integrated model for materials in a fusion power plant: transmutation, gas production, and helium embrittlement under neutron irradiation. Nucl. Fusion 52 (2012) 083019
[27] I.T. Tretiyakov Status of research reactors in Russia and prospects for their development International Symposium on the Peaceful Applications of Nuclear Technology in the GCC Countries, Jeddah 2008
[28] ITER Materials property handbook. Document No. G 74 MA 16
[29] M. Fujitsuka Effect of neutron irradiation on thermal diffusivity of tungsten-rhenium alloys, Journal of Nuclear Materials 283±287 (2000)
[30] Watanbe H and Garner F A Void swelling of pure copper, Cu-5Ni and Cu-5Mn alloys irradiated with fast neutrons. Journal of Nuclear Materials 212-215 (1994) 370-374.
[31] Singe B H et al Void swelling in copper and copper alloys irradiated in fission neutrons, Journal of nuclear materials 191-194 (1992) 1172-1176
[32] Garner F A, Hamilton M L, Shikama T, Edwards D J and Newkirk J W 1992 Response of solute and precipitation strengthened copper alloys at high neutron exposure J. Nucl. Mater. 191–94 386–90
[33] M R Gilbert J-C Sublet, Handbook of activation, transmutation, and radiation damage properties of the elements simulated using FISPACT-II & TENDL-2014; Nuclear Fission plants (HFR focus) http://www.ccfe.ac.uk/assets/documents/easy/Handbook_HFR_UKAEA(15)32.pdf
[34] M Kamaya, M Kawakubo, A procedure for determining the true stress–strain curve over a large range of strains using digital image correlation and finite element analysis, Mechanics of Materials 43 (2011) 243–253
[35] B.N. Singh, J.F. Stubbins, P. Toft. The influence of neutron irradiation on the fatigue performance of OFHC copper and a dispersion strengthened copper alloy Journal of Nuclear Materials 275 (1999) 125±137
[36] ITER SDC-IC Appendix A G 74 MA 8 01-05-28 W 0.2 2012
[37] Tahtinen S et al, Effect of neutron irradiation on fracture toughness behaviour of copper alloys, Journal of Nuclear Materials 258-263 (1998) 1010-1014
[38] M. Li et al. Tensile and fracture toughness properties of neutron-irradiated CuCrZr, Journal of Nuclear Materials 393 (2009) 36–46
[39] Li, M. and J.F. Stubbins, Evaluation of irradiation effect on fatigue performance of copper alloys for high heat flux applications. Fusion Science and Technology, 2003. 44: p. 186-190.
[40] Fabritsieve and Pokrovsky Neutron Irradiation induced High Temperature embrittlement of pure copper Plasma devises and Operations 1997 Vol5 pp133-141
[41] Singh Edwards Horsewell Riso-R-839(EN).pdf
[42] Zinkle S Gibson L.T, Electrical Conductivity And Tensile Properties Of Copper And Oxide Dispersion Strengthened Copper Alloys Following Hfir Irradiation To 13 Dpa At 200 And 400"C – Fusion Materials Semiannual Progress Report For The Period Ending December 31, 1999
[43] https://fispact.ukaea.uk/documentation-2/reports/
[44] Zinkle Copper Alloys For High Heat Flux Structure Applications Nuclear Fusion Supll Atomic And Plasma-Material Interaction Data For Fusion (suppl. to journal of nuclear fusion V5 1994)
[45] Strible F C, Cady J R , "Internal friction in copper subjected to neutron irradiation and fatigue", J. Appl. Phys. 43 (1972) pp.417-424 https://doi.org/10.1063/1.1662305 (to be obtained)
[46] Gorynin I.V et all Effects of neutron irradiation on properties of refractory materials Journal of Nuclear materials 1919-194 (1992) 421-425
[47] Habainy et al, Mechanical properties of tungsten irradiated with high-energy protons and spallation neutron, Journal of nuclear materials 514 (2019) 189-195
[48] Garison LM et al, Mechanical properties of single-crystal tungsten irradiated in a mixed spectrum fission reactor, Journal of Nuclear Materials 518 (2019) 208-225
[49] Katoh Y etal Response of unalloyed tungsten to mixed spectrum neutrons Journal of Nuclear Materials 520 (2019) 193=207
[50] F. Gillemot, M. Horvath, G. Uri, A. Simonits, Neutron Irradiation Effects on Physical and Mechanical Properties of Tungsten, Final Report on TW!-TWP/TU3, HAS, Hungary, 2004
[51] Gaganidze E MAT-1.2.1-T008-D001 – Material Handbook on Tungsten (KIT) Report EUROfusion IDM reference No. 2MX5EF
[52] www.kupferinstitut.de
[53] Nuclear Fusion 52 (2012) 08319

# 8 APPENDIX

## 8.1 *Estimation of neutron fluence per dpa in Tungsten*

The FISPACT handbook [33] provides results of simulation studies of the effect of irradiation on elements (H to Bi) in terms of transmutation and activation for various neutron spectra representative of current fission machine types and anticipated fusion machines. The simulations also determines the expected equivalent dpa for each element for a given fluence which allows factors to be calculated to convert fluence to expected dpa for each material and reactor type. For example: for the HFR Petten spectrum simulation, the determined fluence level of 5.3 x $10^{14}$ n/cm²/s leads to a calculated damage level value of ~2dpa/yr in Tungsten and 4dpa/yr in copper. This equates to a conversion factor of 8.36 x $10^{21}$ n/cm²/dpa for Tungsten and 4.18 x $10^{21}$ n/cm²/dpa for copper.

By comparison, for a fast-breeder reactor (FBR), the determined flux for this system type is 2.376 x $10^{15}$ n/cm²/s with an equivalent dpa for tungsten of 8dpa/year, (conversion factor of 6.56 n/cm²/dpa). For PWRs the respective values are 3.25 × $10^{14}$ n cm−2 s−1 and 1dpa (conversion factor of 10.2 x $10^{21}$ n/cm²/dpa).

The above suggests that the conversion factor for all fission machines could be expressed as 8 ±2 x $10^{21}$ n/cm²/dpa For the purposes of this paper, if the irradiation spectrum information is not specified, an approximate value of 0.8x$10^{22}$ n/cm²/dpa is used .

## 8.2 *Method of determining true stress strain from test data displaying apparent strain softening*

In order to determine the true stress strain characteristic from published test data of engineering stress vs engineering strain with apparent strain softening , a test piece geometry is postulated based on existing standard design as shown in Figure 44. The model is supplied with a postulated true stress strain characteristic (e. g elastic perfectly-plastic as shown in Figure 45) and the tensile test is simulated by applying a fixed extension to the sample end sections. The simulated "engineering stress" is determined from the calculated force divided by the nominal gauge diameter, and the simulated engineering strain from the change in sample gauge length divided by the original length. The resulting stress strain characteristic is compared with the observed published stress strain curve as shown in Figure 47. The postulated input true stress strain characteristic is modified (in both amplitude and shape) until the simulated engineering stress strain curve matches the test result.

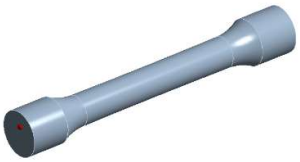

Figure 44 Model used for test response simulation: Central bar diameter 20mm parallel length 110mm

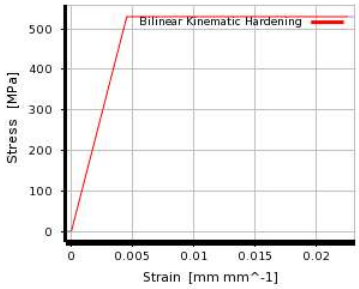


Figure 45 ANSYS graphical display of bilinear material model data entered

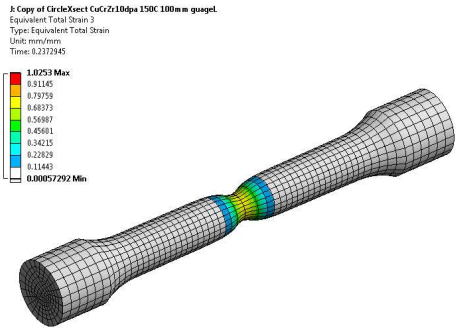


Figure 46 resulting necked response from simulation with 1:1 displacement scaling

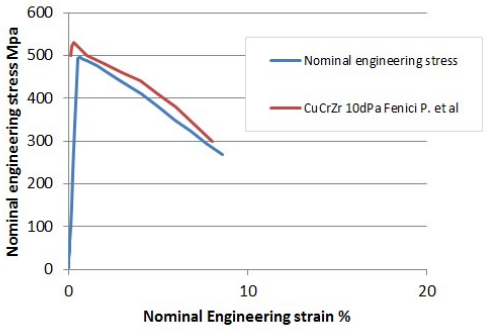


Figure 47 Nominal engineering stress and strain response (in blue) evaluated from the elastic perfectly plastic FE model using a 150mm gauge length. This is shown in comparison with published test data (red curve)

### 8.3 *Materials properties and limit data*

Table 5 Summary of properties of considered materials at selected temperatures (taken from[36]) with thermal conductivity correction for 13dpa irradiation

| | Temperature (˚C) | Coefficient of Thermal Expansion (1/˚C) | Young's Modulus (MPa) | Unirradiated Thermal Conductivity (W /mm K) | Irradiated Thermal Conductivity (W /mm K) | Poisson's ratio |
|---|---|---|---|---|---|---|
| Copper | 20 | 1.68E-05 | 117000 | 0.401 | 0.341 | 0.33 |
| | 400 | 1.82E-05 | 98000 | 0.374 | 0.318 | 0.33 |
| CuCrZr | 20 | 1.67E-05 | 127500 | 0.318 | 0.032 | 0.33 |
| | 450 | 1.82E-05 | 110000 | 0.347 | 0.035 | 0.33 |
| Tungsten | 20 | 4.50E-06 | 398000 | 0.173 | 0.08 | 0.28 |
| | 1200 | 4.98E-06 | 356000 | 0.105 | 0.105 | 0.28 |

Table 6 Cyclic rule assessment Chaboche model parameter values for copper and CuCrZr elasto-plastic kinematic hardening model.

| | Copper | | | | CuCrZr | | | |
|---|---|---|---|---|---|---|---|---|
| | temperature °C | Yield Stress (MPa) | Material Constant C1 (MPa) | Material Constant γ1 | temperature °C | Yield Stress (MPa) | Material Constant C1 (MPa) | Material Constant γ1 |
| Unirradiated | 20 | 58 | 1500 | 5 | 20 | 220 | 333 | 2 |
| | 80 | 55 | 1500 | 6 | 350 | 190 | 333 | 10 |
| | 400 | 18 | 1500 | 12 | | | | |
| | 600 | 8.5 | 1500 | 18 | | | | |
| | 800 | 4 | 1500 | 24 | | | | |
| Irradiated | 20 | 175 | 1500 | 4 | 20 | 300 | 6000 | 60 |
| | 80 | 150 | 1500 | 4 | 350 | 230 | 6000 | 60 |
| | 150 | 125 | 1500 | 4 | | | | |
| | 250 | 80 | 1500 | 6 | | | | |
| | 400 | 30 | 1500 | 12 | | | | |
| | 600 | 8.5 | 1500 | 18 | | | | |
| | 800 | 4 | 1500 | 24 | | | | |

Table 7 Monotonic rule assessment Chaboche model parameter values for Copper and CuCrZr elasto-plastic kinematic hardening models.

| | Copper | | | | CuCrZr | | | |
|---|---|---|---|---|---|---|---|---|
| | temperature °C | Yield Stress (MPa) | Material Constant C1 (MPa) | Material Constant γ1 | temperature °C | Yield Stress (MPa) | Material Constant C1 (MPa) | Material Constant γ1 |
| Unirradiated | 20 | 58 | 1500 | 5 | 20 | 220 | 333 | 2 |
| | 80 | 55 | 1500 | 6 | 350 | 190 | 333 | 10 |
| | 400 | 18 | 1500 | 12 | | | | |
| | 600 | 8.5 | 1500 | 18 | | | | |
| | 800 | 4 | 1500 | 24 | | | | |
| Irradiated | 20 | 350 | 250 | 4 | 20 | 290 | 6000 | 4500 |
| | 80 | 300 | 250 | 4 | 150 | 265 | 6000 | 4500 |
| | 150 | 250 | 250 | 4 | 200 | 237 | 500 | 50 |
| | 250 | 80 | 1500 | 6 | 250 | 210 | 333 | 5 |
| | 400 | 30 | 1500 | 12 | 400 | 180 | 333 | 5 |
| | 600 | 8.5 | 1500 | 18 | | | | |
| | 800 | 4 | 1500 | 24 | | | | |

Table 8 Limit data for Irradiated CuCrZr and Copper

| | |
|---|---|
| CuCrZr True strain at rupture) | see Figure 21 Minimum total strain at rupture data provided by ITER [36]for dpa in the range 0.3 to 5.0 (from test 0 2.5dpa) and proposed best fit curve for IAP exhaustion of ductility rule.) |
| CuCrZr Fracture toughness | see Figure 27 proposed fracture toughness characteristic for the IAP assessment of irradiated Solution annealed + aged CuCrZr. Figure 27 proposed fracture toughness characteristic for the IAP assessment of irradiated Solution annealed + aged CuCrZr. |
| Copper True strain at rupture | – see Figure 29 Total elongation of irradiated copper as measure by Fabritsiev [40] for a range of test temperatures at an estimated 2 dpa. (Bor-60 reactor) |

Table 9 Fatigue data for CuCrZr for both Irradiated and unirradiated.

| | CuCrZr design curve [22] |
|---|---|
| Cycles | total strain range % |
| 10 | 2.29 |
| 40 | 1.395 |
| 100 | 1.026 |
| 400 | 0.672 |
| 1000 | 0.526 |
| 4.00E+03 | 0.376 |
| 1.00E+04 | 0.308 |
| 4.00E+04 | 0.2233 |
| 1.00E+05 | 0.1852 |